PROTEINS: Structure, Function, and Genetics 15:147–176 (1993)

# Crystal Structure of CTP-Ligated T State Aspartate Transcarbamoylase at 2.5 Å Resolution: Implications for ATCase Mutants and the Mechanism of Negative Cooperativity

**Richard P. Kosman,[1,2] J. Eric Gouaux,[3] and William N. Lipscomb[1]**

[1]*Department of Chemistry, Gibbs Chemical Laboratory, Harvard University, Cambridge, Massachusetts 02138,*
[2]*Harvard Medical School, Health Sciences and Technology Division, Boston, Massachusetts 02115, and*
[3]*Department of Chemistry, Massachusetts Institute of Technology, Cambridge, Massachusetts 02139*

*ABSTRACT* **The X-ray crystal structure of CTP-ligated T state aspartate transcarbamoylase has been refined to an *R* factor of 0.182 at 2.5 Å resolution using the computer program X-PLOR. The structure contains 81 sites for solvent and has rms deviations from ideality in bond lengths and bond angles of 0.018 Å and 3.722°, respectively. The cytosine base of CTP interacts with the main chain carbonyl oxygens of *r*Tyr-89 and *r*Ile-12, the main chain NH of *r*Ile-12, and the amino group of *r*Lys-60. The ribose hydroxyls form polar contacts with the amino group of *r*Lys-60, a carboxylate oxygen of *r*Asp-19, and the main chain carbonyl oxygen of *r*Val-9. The phosphate oxygens of CTP interact with the amino group of *r*Lys-94, the hydroxyl of *r*Thr-82, and an imidazole nitrogen of *r*His-20. Recent mutagenesis experiments evaluated in parallel with the structure reported here indicate that alterations in the hydrogen bonding environment of the side chain of *r*Asn-111 may be responsible for the homotropic behavior of the pAR5 mutant of ATCase. The location of the first seven residues of the regulatory chain has been identified for the first time in a refined ATCase crystal structure, and the proximity of this portion of the regulatory chain to the allosteric site suggests a potential role for these residues in nucleotide binding to the enzyme. Finally, a series of amino acid side chain rearrangements leading from the *R*1 CTP allosteric to the *R*6 CTP allosteric site has been identified which may constitute the molecular mechanism of distinct CTP binding sites on ATCase.**



**Key words: X-ray crystallography, pAR5 mutant, allosteric enzyme, ligand-induced negative cooperativity, alternative amino acid conformations, coordinate error**



## INTRODUCTION

Aspartate transcarbamoylase from *Escherichia coli* (ATCase, EC 2.1.3.2) is a cooperative enzyme which catalyzes the reaction between L-aspartate and carbamoyl phosphate, the first committed step in the biosynthesis of pyrimidines in *E. coli*.[1] The products of the reaction are inorganic phosphate and *N*-carbamoyl-L-aspartate,[2] the latter continuing through the pyrimidine biosynthetic pathway to uridine 5′-triphosphate (UTP) and (especially relevant here) cytidine 5′-triphosphate (CTP). The enzyme has been the subject of a plethora of recent reviews, three of which have focused on the current approach to elucidating the enzyme's structure and function which involves combining the results of crystallography with molecular biology.[3–5] Two general mechanisms have evolved to regulate pyrimidine production in *E. coli* (for a review see Kantrowitz et al.[6,7]). The first occurs at the level of transcription of ATCase mRNA and involves the operation of a repressor mechanism at high concentrations of uracil.[8] The other form of control involves alterations in ATCase activity, and this enzymatic mechanism encompasses homotropic activation by L-aspartate and feedback inhibition and heterotropic activation by CTP and adenosine 5′-triphosphate (ATP), respectively. Allosteric inhibition in *E. coli* involves pyrimidine derivatives of which CTP is the most effective.[9] Although UTP has minimal effects on ATCase activity when acting alone,[10] it synergizes the inhibition observed with CTP.[11] ATP, the

Received April 10, 1992; revision accepted June 8, 1992.
Address reprint requests to W. N. Lipscomb, Department of Chemistry, Harvard University, 12 Oxford Street, Cambridge, MA 02138.
The ensemble of coordinates produced during refinement and utilized to estimate the minimal uncertainties in the atomic positions of ATCase (8 structures) and the final, refined CTP-ligated ATCase structure which represents the substance of this report (9 structure total) were deposited in the Protein Data Bank, Building 555—Chemistry Department, Brookhaven National Laboratory, Upton, NY 11973.

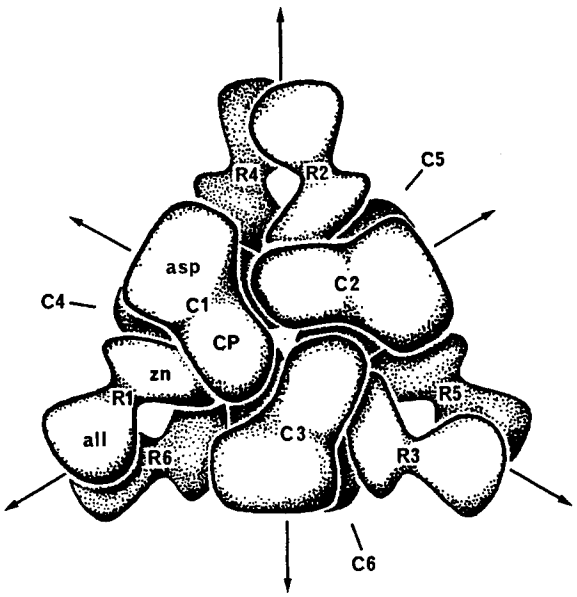


Fig. 1. A view of the ATCase holoenzyme parallel to the crystallographic 3-fold rotation axis. This diagram illustrates the general relationship between the two catalytic trimers (shown stacked on top of each other in the plane of the page) and the three regulatory dimers. The domains of the individual catalytic and regulatory chains are also delineated—the catalytic chain is divided into aspartate (asp) and carbamoyl phosphate (CP) domains and the regulatory chain is divided into zinc (zn) and allosteric (all) domains. The zn domain contains a zinc ion coordinated to four cysteine residues, and the all domain possesses the binding site for nucleoside triphosphate effectors.

end product of the purine pathway, heterotropically activates ATCase.[9,10] Both CTP and ATP compete for the same binding sites on ATCase which are located about 60 Å from the catalytic sites.[12,13]

The ATCase holoenzyme (MW 310,000) is composed of six catalytic ($c$) polypeptide chains (MW 33,000 each) and six regulatory ($r$) chains (MW 17,000 each).[14,15] The catalytic polypeptide chains aggregate to form two catalytic trimers ($2c_3$), and the regulatory chains assemble to create three regulatory dimers ($3r_2$).[14] The arrangement of subunits is depicted in Figure 1.* The catalytic subunits ($c_3$) catalyze the carbamoylation of L-aspartate without exhibiting the homotropic cooperativity observed in the intact enzyme, and the regulatory subunits ($r_2$) bind nucleoside triphosphates without exhibiting any catalytic behavior.[16]

Several early experiments first identified contracted (**T**) and expanded (**R**) forms of the enzyme.† Sedimentation velocity experiments demonstrated that the sedimentation coefficient of ATCase decreases in the presence of carbamoyl phosphate/succinate[17] or *N*-(phosphonacetyl)-L-aspartate (PALA),[18] substrate analogues or bisubstrate analogue, respectively. X-ray solution scattering studies predicted a 10 to 12 Å expansion of the molecule upon binding of PALA,[19] and single crystal X-ray diffraction of **R** state crystals predicted a molecular expansion of the **R** state relative to the **T** state of approximately 8 Å.[20,21]

The **T** state has a lower affinity for substrates and is less catalytically active than the **R** state of the enzyme.[22] At pH 7.0 in the absence of ligands the equilibrium constant $L=[\mathbf{T}]/[\mathbf{R}]$ is approximately 250,[22] allowing structural analysis with crystallography to proceed on virtually uncontaminated **T** state of the enzyme. Analogous work on the **R** state was first accomplished with PALA,[23] which at concentrations as low as one molecule of PALA/ATCase holoenzyme induces the **T** → **R** transition.[24] Currently, crystal structures are available for the unligated **T** state of ATCase,[25–27] the CTP-bound **T** form of ATCase,[25,27,28] the ATP-bound **T** form of ATCase,[27] the PALA-bound **R** form of ATCase,[29,30] the carbamoyl phosphate/succinate-ligated **R** state,[31] the phosphonoacetamide (PAM)-bound **T** and PAM/malonate-bound **R** states,[32] and the PAM/malonate/CTP-bound and PAM/malonate/ATP-ligated **R** states.[33] The quaternary changes marking the **T** → **R** transition include a net rotation of 12° of one $c_3$ trimer relative to the other (to a more eclipsed position of the two trimers), a clockwise rotation of 15° by the $r_2$ dimers around their 2-fold axes, and an expansion of 11 Å along the 3-fold axis of the molecule.[29,34]

In addition to the recent crystallographic research aimed at precisely delineating the interactions of the substrates and substrate analogues with residues implicated in binding and catalysis[31,32] and work germane to an appreciation of the interactions of nucleoside triphosphate ligands with the enzyme,[27,28,33] another major focus of recent X-ray structural work has been to correlate the biochemical behavior of ATCase mutants with structural information derived from X-ray crystallography in order to delineate the homotropic and heterotropic regulatory pathways of the enzyme.‡,[3,5] The first

*The asymmetric unit of the *P*321 crystal form of ATCase consists of two catalytic chains (one from each of the two catalytic trimers) related by a regulatory dimer. These four chains have traditionally been given either letter designations (A–D) or alphanumeric designations (*C*1, *R*1, *C*6, and *R*6) in which the A chain corresponded with chain *C*1, the B chain corresponded with chain *R*1, and so on. The alphanumeric designations will be employed throughout this report.

†**T** refers to the "tense" conformational state of aspartate transcarbamoylase defined by the unit cell dimensions of the crystal form of the enzyme. It crystallizes in the space group *P*321 with the approximate unit cell dimensions $a\approx122$ Å and $c\approx142$ Å. **R** refers to the "relaxed" conformation of aspartate transcarbamoylase which, like the **T** conformational state, crystallizes in the space group *P*321. However, the approximate unit cell dimensions of the **R** state are $a\approx122$ Å and $c\approx156$ Å. The relevant functional and molecular differences between these two states are discussed in the text.

‡The notation employed to name a mutant throughout this report will consist of the native enzyme amino acid residue and sequence number followed by an arrow and the residue type

characterized mutant of ATCase bearing a modification in the regulatory chain was pAR5.[36–38] This mutant is the result of the replacement of the eight carboxy-terminal amino acids of ATCase (Ser-His-Asn-Val-Val-Leu-Ala-Asn) with a new sequence of six residues (Tyr-Thr-Lys-Leu-Ala-Leu).[37,38] pAR5 ATCase lost homotropic cooperative interactions and CTP inhibition, though enzymatic activation by ATP remained intact.[38] Subsequent X-ray solution scattering studies on pAR5 conducted by Cherfils et al.[39] indicated that the mutant adopts a conformation consistent with an intermediate between the **T** and **R** states. The properties of the mutant and the results of parallel energy minimizations on the mutant and native forms of ATCase[39] suggested that the alterations in homotropic and heterotropic behavior observed by Ladjimi et al.[38] were the manifestation of alterations in the *C*1–*R*4 interface (which is ruptured in the allosteric transition from the **T** → **R** state[29]) and in *r*Lys-28 (in the vicinity of the allosteric binding site), respectively.

The present study was initiated by the belief that higher resolution, more complete data, and refinement by simulated annealing[40] would serve to better refine the orientation of CTP in the allosteric site of the **T** form of the enzyme, to better explore amino acid side chain interactions in the wild-type and mutant forms (especially pAR5) of the enzyme, and to locate the first seven residues of the regulatory chains of ATCase which have been implicated in the binding of nucleotides and, as a consequence, implicated in the heterotropic effects.[25,27,41,42] In addition, the higher resolution and more complete data afforded an opportunity to explore the asymmetry in CTP-ligated ATCase in more detail—specifically, the molecular details of the two separate classes of CTP binding sites on ATCase.[43,44] Interestingly, binding studies of carbamoyl phosphate with ATCase have revealed the existence of two sets of distinct binding sites for the substrate.[45] More recent work on the synergistic inhibition of ATCase in the presence of CTP and UTP[11] demonstrated that this heterogeneity in CTP binding persists in the presence of UTP. Unfortunately, it is difficult to ascertain in these studies whether this presumed asymmetry is *inherent* in the native form of ATCase or whether it is a *consequence* of ligand binding,[41,43,45–47] though the two forms of asymmetry are not mutually exclusive. In this highest resolution X-ray crystal structure of the CTP-ligated **T** form of aspartate transcarbamoylase (data collection to 2.4 Å and structure refinement to 2.5 Å), pertinent aspects of the structure are described, and from this structure models are developed to account for the significance of the orientation of the first seven residues of the regulatory chains of ATCase, for the functional behavior of the pAR5 mutant of the enzyme, and for the molecular basis of the high and low affinity CTP binding sites on the regulatory dimer of the enzyme.

## MATERIALS AND METHODS

Aspartate transcarbamoylase was isolated, purified, and crystallized in the presence of CTP as previously described for the *c*Tyr-240 → Phe mutant.[48] The crystals grew in the space group *P*321 with unit cell parameters $a = 122.13$ Å and $c = 142.51$ Å at pH 5.8. X-ray diffraction data were collected to 2.4 Å resolution at the Biotechnology Resource, University of Virginia, on the multiwire area X-ray diffractometer[49] in the same manner as reported previously.[48]

Data were recorded from six crystals. Lorentz and polarization corrections were performed on all intensity data. The method of Fox and Holmes[50] as implemented in the CCP4 crystallographic program package was employed to scale all reflections associated with each individual crystal with data from Kim et al.[28] (the reference data set) and then the data associated with each individual crystal were merged without the reference data set. Subsequently, scaled data from all six of the crystals were scaled together with the standardized data set but once again merged without the standardized data set. The data from one of the crystals did not scale well with the other crystals even after swapping *h* and *k* indices. This crystal was assumed to either have been twinned or to have slipped during data collection, and the data from it were discarded. The scaling and reduction of the final five crystals involved 169,691 observations of 35,204 independent reflections with $I \geq 2\sigma(I)$. These data are 82% complete in the resolution range 2.5 to 10.0 Å and include approximately 50% more unique reflections than the data associated with the model

which replaced the native amino acid; for example, *c*Tyr-240 → Phe indicates that a tyrosine residue (sequence number 240 of the catalytic chain) was replaced with a phenylalanine. The letter *c* or *r* preceding the residue type and number indicates whether the residue is a constituent of the catalytic or *r*egulatory chain.

Although site-directed mutagenesis studies on ATCase will be cited throughout this report to bolster observations made on the basis of the crystal structures of the enzyme, the reader should be cognizant of the limitations of attempting to extrapolate wild-type function from that of a mutant. For example, although the results of site-directed mutagenesis studies on proteins have often been interpreted to reflect localized differences in the structures of wild-type and mutant proteins, Karplus and co-workers[35] have shown that such assumptions are not without hazard. The analysis of the free energy differences of the oxy and deoxy forms of the Asp G1(99)β → Ala mutant of hemoglobin with molecular dynamics free energy simulations demonstrated that although hydrogen bonds to residues identified by the X-ray structures [Tyr C7(42)α and Asn G4(97)α] were a significant portion of the free energy change when the deoxy and oxy forms of the mutant were compared, the solvent and other interchain and intrachain interactions were also important.

structure which was used to refine it.[28] The final $R_{merge}$[§] was 0.097.

The refinement of the current structure began with the model of Kim et al.[28] as the starting point. All solvent molecules, both CTP molecules, and all partially occupied residues were deleted from the coordinate file of the model structure. All occupancies were set to 1.0, and all reflections with $I/\sigma(I) \geq 2$ were given a weight of 1.0. All other reflections were omitted from the refinement. The initial rounds of refinement were carried out with X-PLOR[40,51] installed on the CRAY X-MP at the Pittsburgh Supercomputing Center. Fifty cycles of positional refinement in the resolution range 2.4 to 6.0 Å were performed using the algorithm described by Powell[52] as it is incorporated into X-PLOR.[51] In this resolution range (2.4–6.0 Å), the data are 75% complete. The zinc–sulfur bond lengths and angles as well as the corresponding parameters for CTP were determined and employed as has already been described.[33] The charges on lysines, aspartates, glutamates, and arginines were turned off throughout the refinement[51] to prevent the introduction of discrepant electrostatic energy terms. The initial $R$ factor[¶] was 0.316 and the $R$ factor at the conclusion of 50 cycles was 0.236. The root mean squared (rms) deviations in bond angles and bond lengths[51] (see the footnote to Table II) from their ideal values were 4.374° and 0.021 Å, respectively. Twenty cycles of subsequent temperature ($B$) factor refinement reduced the $R$ factor to 0.224.

Electron density maps based on these refined coordinates were created with a fast Fourier transformation program.[53,54] Maps with coefficients $(2|F_o| - |F_c|)e^{i\alpha_{calc}}$ and $(|F_o| - |F_c|)e^{i\alpha_{calc}}$ were used to determine the positions of CTP and solvent. All interactive modeling was performed on an Evans and Sutherland PS300 interfaced with a VAX 11/780 running the software program FRODO.[55,56] As a starting point, the coordinates of all 950 water molecules and the two CTP molecules from the Kim et al.[28] structure were added to the refined coordinate file. Two sets of criteria were established for the maintenance of a solvent site. The crystallographic criteria involved visualization of peak density at 0.20 electrons/Å$^3$ (3.4$\sigma$) in the $(|F_o| - |F_c|)e^{i\alpha_{calc}}$ map and the appropriate geometry and fit of density at a contour level of 2.5$\sigma$ or higher in the same map, where $\sigma$ represents the standard deviation in $\rho_o$. The chemical criteria for solvent[28] demanded that all donor/acceptor pairs had to be between 2.4 and 3.2 Å apart and that each water molecule had to belong to a traceable network of hydrogen-bonded water molecules back to the surface of the protein. Ninety-three solvent molecules fulfilled these criteria. The conformation warranted by the density of both CTP molecules was in accord with the assignment of the *anti* conformation of the pyrimidine ring relative to the ribose ring.

The entire protein structure was reviewed for its fit in $(2|F_o| - |F_c|)e^{i\alpha_{calc}}$ map density, and individual amino acid side chains were adjusted to provide the best compromise between the conformation warranted by the electron density and favorable values of $\chi^1$ and $\chi^2$ angles observed in amino acid side chains of proteins.[57] The density in the vicinity of the *c*80s loop indicated the necessity of a reposition of residues 76–85 of chain *C*1 and residues 76–86 of *C*6 without alterations in the connectivity of the chains. Significant and contiguous electron density in the region away from Gln-8 and toward the amino-terminus in both regulatory chains of the asymmetric unit permitted the initial tracing of residues 1–7 of the regulatory chain (though *R*6 residues 1–7 were deleted at the conclusion of refinement due to the suboptimal electron density associated with their final, refined positions (see Results and Discussion)). Other recent refinements of ATCase bound with various effectors and in both the **T** and **R** states lacked adequate electron density to assign positions to the first seven residues of the regulatory chains,[27,28,30,33] though it is clear that extension of the regulatory chain beyond Gln-8 and toward the amino-terminus places residues in the vicinity of the nucleotide binding site and is consistent with a potential role for those residues in the heterotropic mechanism and/or the binding of nucleotides.

Since refinement with X-PLOR[40,51] sets a default double protonation state for histidines and this double protonation can introduce discrepant van der Waals and/or electrostatic energy terms,[58] the crystallographic and chemical environment of all histidines in the asymmetric unit of ATCase were reviewed and protonation states were assigned (Table I). In addition, the chemical environment of all asparagine and glutamine side chains was inspected and the terminal amide group was adjusted to yield the maximum number of hydrogen bonds with neighboring residues.

The $B$ factors for all of the atoms added to the trial structure during this round of interactive model building (i.e., solvent, *r*1–7, and CTP) were set to 20.0 Å$^2$ for the next rounds of molecular refinement. The structure was subjected to another 90 cycles of Powell minimization with X-PLOR[40,51] installed on a VAXstation II. The resolution limits were set to 2.4 and 10.0 Å in order to ensure that all reasonably well ordered solvent data were included in the re-

$$R_{\text{merge}} = \frac{\sum_{hkl}\sum_{i} |I_{mean} - I_i|}{\sum_{hkl}\sum_{i} I_i}$$

$$R \text{ factor} = \frac{\sum_{hkl} ||F_o| - |F_c||}{\sum_{hkl} |F_o|}$$

**TABLE I. Protonation States Assigned to Histidine Residues in CTP-Ligated T State Aspartate Transcarbamoylase at pH 5.8***

| | *C1* | | | *C6* | |
|---|---|---|---|---|---|
| Residue | $N^{\delta 1}$ | $N^{\epsilon 2}$ | Residue | $N^{\delta 1}$ | $N^{\epsilon 2}$ |
| 8 | − | + | 8 | − | + |
| 41 | − | + | 41 | + | + |
| 64 | + | + | 64 | + | + |
| 106 | − | + | 106 | − | + |
| 134 | − | + | 134 | − | + |
| 156 | + | + | 156 | + | + |
| 170 | + | + | 170 | + | + |
| 212 | + | − | 212 | + | + |
| 255 | + | + | 255 | + | + |
| 265 | − | + | 265 | − | + |
| 282 | − | + | 282 | − | + |
| | *R1* | | | *R6* | |
| 3 | + | + | 3† | | |
| 20‡ | + | + | 20 | + | + |
| 117 | + | + | 117 | + | + |
| 147 | + | + | 147 | − | + |

*"+" is used to denote the presence of a proton on the designated imidazole nitrogen while "−" is used to denote the absence of a proton on the designated nitrogen.
†Since this residue is a constituent of the first seven residues of *R*6 which could not be unequivocally positioned in electron density in the structure after refinement was complete, its assigned protonation state has been omitted from the table.
‡The protonation state reported for this residue is consistent with the chemical environment of this side chain *subsequent* to simulated annealing refinement.[40,51]

finement. In this resolution range (2.4–10.0 Å), the data are 77% complete. The initial *R* factor was 0.251, and at the conclusion of these rounds of refinement it was 0.217. The rms deviations of bond angles and lengths were 4.093° and 0.020 Å, respectively. Another 31 cycles of restrained *B* factor refinement with X-PLOR[40,51] performed on a VAXstation III yielded an *R* factor of 0.199.

The coordinates were then subjected to refinement by simulated annealing.[40,51] In addition to the coordinates which represent the final structure of CTP-ligated ATCase, coordinate files were output in 250 step increments during the molecular dynamics equilibration calculations and then subjected to rapid and slow cooling protocols followed by 50 final cycles of Powell minimization. This procedure yielded a series of structures from which better estimates of coordinate error could be made and applied to ATCase for future studies (see Fig. 2 and Results and Discussion). Statistics for the structures derived using this method are summarized in Table II. All refinements which involved molecular dynamics employed resolution limits of 2.5–10.0 Å (82% complete data) due to the paucity of data in the resolution range 2.4 to 2.5 Å and in order to decrease the central processing time for the refinements. The refinements were performed either on the Cray Y-MP at the Pittsburgh Supercomputing Center or on a Digital DECstation 3100. The coordinates which had been equilibrated for 1,000 steps and cooled using the slow procedure were subjected to a final 15 rounds of restrained *B* factor refinement. These coordinates represent the complete, refined structure of T state CTP-ligated ATCase. The final *R* factor is 0.182 (Table III), and the rms deviations from ideality of bond lengths, bond angles, and ω angles are 0.018 Å, 3.72°, and 5.58°, respectively.

The stereochemistry of the polypeptide main chain as described by (ϕ,ψ) is displayed in Figure 3 in a plot modeled after the analysis by Ramachandran et al.[59] Of the amino acids with (ϕ,ψ) which differed by 30° or more from the allowed regions of the Ramachandran plot[59] only Leu-267 of chains *C*1 and *C*6 and Leu-107 of chain *R*6 were in strong electron density (unambiguously positioned at 1.5σ in a $(2|F_o| - |F_c|)e^{i\alpha_{calc}}$ map) and had low thermal parameters ($B < 25$ Å$^2$). These results are very similar to those reported previously[28] in which Leu-267 of chains *C*1 and *C*6 were identified using similar qualitative criteria, though this is the first identification of *R*6 Leu-107 with the criteria delineated above. *C*1 and *C*6 Leu-267 may be constrained to possess unfavorable main chain dihedral angles (and consequently, to fall into a disallowed region of the Ramachandran plot[59]) because they are both preceded and succeeded by proline residues, the peptide link between *c*Leu-267 and *c*Pro-268 assuming the *cis* conformation. *R*6 Leu-107 is located in a hydrophobic pocket formed by residues Leu-76, Tyr-77, Ile-103, Val-106, Phe-125, Val-127, Ile-134, Leu-136, Val-150, and Leu-151—all also belonging to chain *R*6. It is possible that the entropically driven hydro-

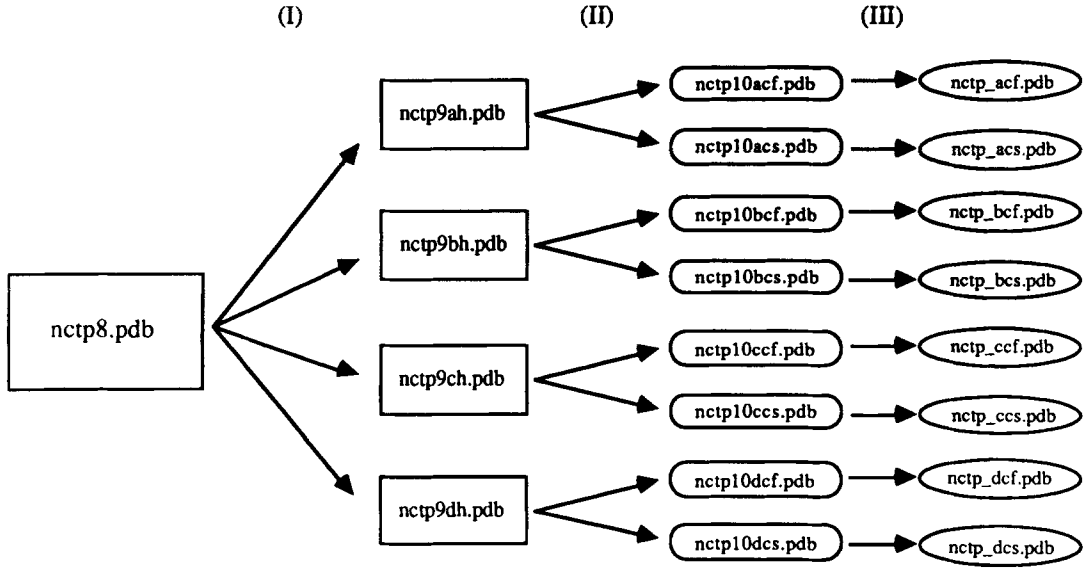


Fig. 2. Schematic of the refinement protocol.[40,51] (I) The four coordinate files labeled nctp9ah.pdb through nctp9dh.pdb represent the output after molecular dynamics equilibration at 2,000 K in 250 step intervals on the nctp8.pdb structure (i.e., nctp9ah.pdb was output after 250 steps of equilibration had been performed, nctp9bh.pdb was output after 500 steps had been performed, etc.). (II) Each set of equilibrated coordinates was then subjected to two cooling procedures. The first involved the fast cooling protocol of simulated annealing (SA) refinement,[40,51] and the second involved the slow cooling protocol of SA refinement.[40,51] (III) All structures were subjected to a final round of Powell minimization.[40,51]

**TABLE II. Overall Statistics for the Refinements**

| | | rms deviation* | | | |
|---|---|---|---|---|---|
| Structure | *R* factor | Bonds (Å) | Angles (°) | Dihedrals (°) | Impropers (°) |
| Initial CTP-ATCase structure | 0.199 | 0.020 | 4.093 | 26.731 | 2.120 |
| CTP-ATCase/acf | 0.191 | 0.018 | 3.742 | 26.736 | 1.769 |
| CTP-ATCase/acs | 0.190 | 0.018 | 3.742 | 26.607 | 1.852 |
| CTP-ATCase/bcf | 0.189 | 0.017 | 3.751 | 26.818 | 1.795 |
| CTP-ATCase/bcs | 0.189 | 0.017 | 3.726 | 26.777 | 1.850 |
| CTP-ATCase/ccf | 0.189 | 0.018 | 3.769 | 26.885 | 1.821 |
| CTP-ATCase/ccs | 0.188 | 0.017 | 3.714 | 26.514 | 1.809 |
| CTP-ATCase/dcf | 0.188 | 0.017 | 3.734 | 26.622 | 1.812 |
| CTP-ATCase/dcs | 0.189 | 0.018 | 3.722 | 26.670 | 1.802 |

*All rms deviations were calculated with respect to ideality and are defined by the following equation:[51]

$$\sigma = \sqrt{\frac{\sum_{i=1}^{N} (x_i - x)^2}{(N)}}$$

where $x_i$ is the experimental value for the particular quantity being considered, $x$ is the accepted value of that quantity, and $N$ represents the number of observations of the particular type (bond distances, angles, etc.) being considered in the calculation.

phobic interaction leads to the energetically unfavorable main chain dihedral angle of *R*6 Leu-107.

Simulated annealing refinement as it is incorporated in X-PLOR employs molecular dynamics to increase the radius of convergence of conventional least squares refinement.[40,51] As a consequence of the extreme conditions (2,000 K) it subjects a structure to, refinement with X-PLOR[40,51] was expected to result in large displacements of solvent. The rms differences in the coordinates of solvent oxygen atoms after positional (Powell) refinement relative to their positions prior to positional refinement were 0.6 Å. Only 9 of the 93 water oxygens moved more than 1.0 Å and the most mobile oxygen atom moved

**TABLE III. *R* Factor as a Function of Resolution for CTP-Ligated T State Aspartate Transcarbamoylase**

| Resolution range (Å) | Number of reflections | *R* Factor |
|---|---|---|
| 4.83–10.00 | 5261 | .1852 |
| 3.91–4.83 | 3240 | .1392 |
| 3.44–3.91 | 4420 | .1575 |
| 3.13–3.44 | 4648 | .1827 |
| 2.91–3.13 | 4374 | .1972 |
| 2.75–2.91 | 4046 | .2163 |
| 2.61–2.75 | 3818 | .2215 |
| 2.50–2.61 | 3245 | .2284 |
| | 33052 | .1819 |

1.4 Å. Equilibration of the structure at 2,000 K and slow annealing resulted in rms differences in solvent oxygen atom coordinates of 2.8 Å relative to the corresponding coordinates prior to this procedure, and one of these oxygen atoms moved 9.2 Å. The interaction distance restraints criterion was relaxed in this review of the structure relative to the one employed earlier in the acceptance of putative solvent sites, though the other criteria were maintained (see above). Specifically, solvent sites were accepted if they permitted hydrogen bond interactions at a distance of 2.4 to 3.5 Å. Using this new criterion and the criteria delineated above, 12 solvent sites were eliminated from the final coordinate file yielding a total of 81 solvent molecules in the crystallographic asymmetric unit.

## RESULTS AND DISCUSSION

### Multiple Conformers and the Quality of the Structure

All previously described T state aspartate transcarbamoylase side chains thought to exist as two

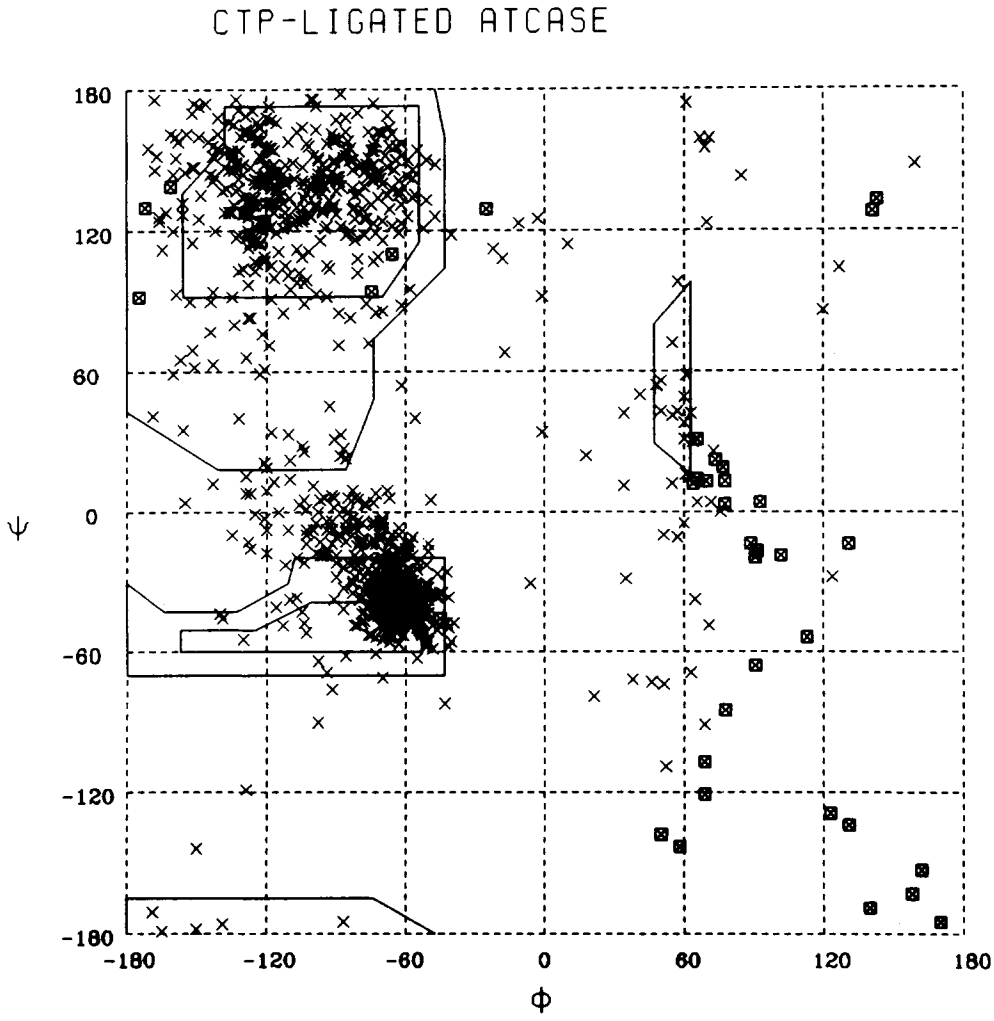


Fig. 3. Ramachandran plot[59] of the amino acid main chain dihedral angles (ϕ,ψ) in the asymmetric unit [926 amino acid residues; 918 (ϕ,ψ) pairs] of *P*321 cytidine 5′-triphosphate-ligated T state ATCase. All glycine residues are indicated by an "X" surrounded by a box.

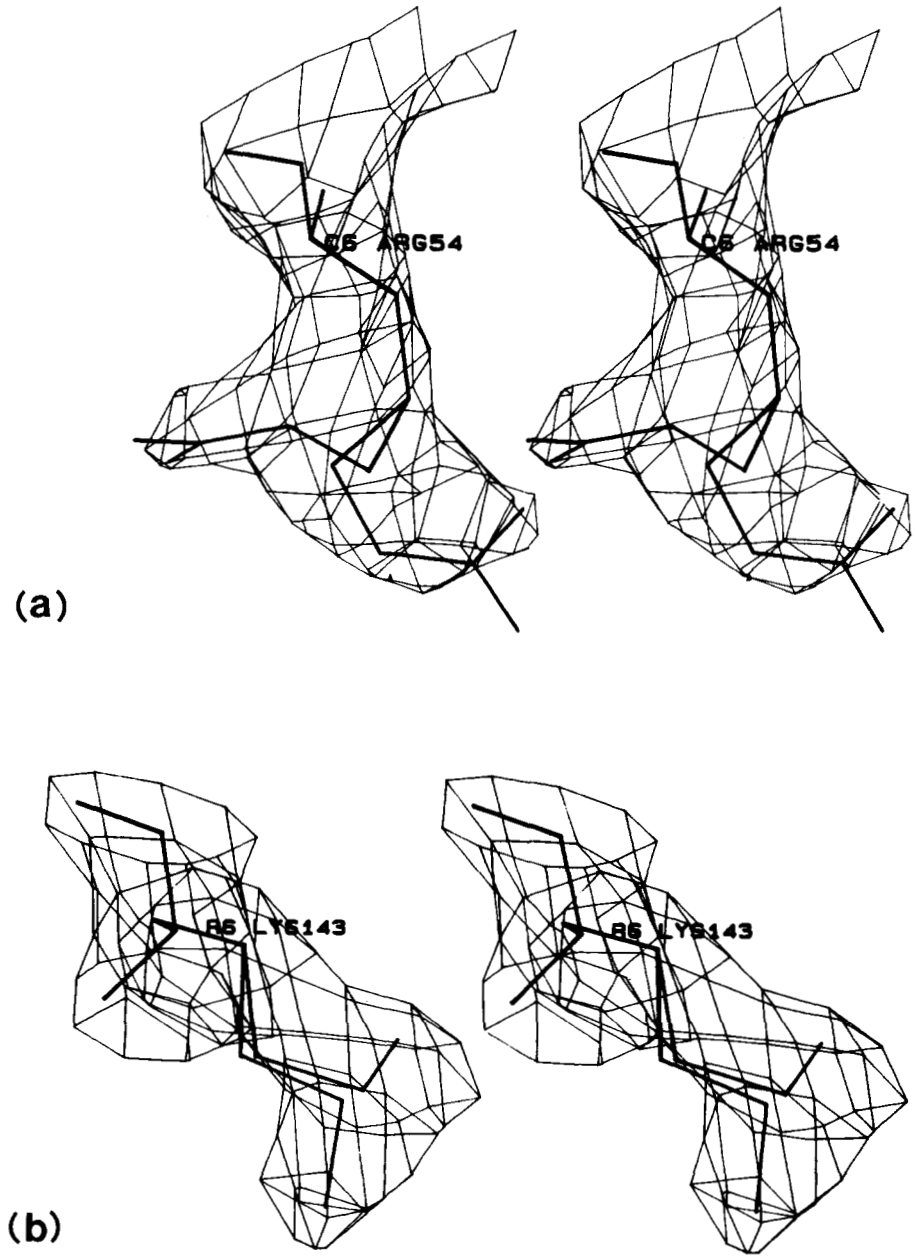


Fig. 4. Stereodiagrams of **(a)** *C*6 Arg-54 and **(b)** *R*6 Lys-143 in which the electron density maps for both residues were calculated with the coefficients $(2|F_o| - |F_c|)e^{i\alpha_{calc}}$ and contoured at 1.3$\sigma$.

conformers[28] were analyzed to resolve any ambiguities in their putative orientations. The criteria used to determine whether or not a particular amino acid side chain existed as alternate conformers were as follows. First, the electron density had to support the existence of two distinct conformations of the side chain. This criterion was satisfied if the amino acid side chain had two clearly demarcated and uninterrupted paths in the $(2|F_o| - |F_c|)e^{i\alpha_{calc}}$ map at a contour level of at least 1.0$\sigma$ and if these paths were separated by an area of absent density as viewed in the same electron density map. Of the 25 residues in alternate conformers identified by Kim et al.,[28] only six had electron density which fulfilled the density criterion of this report. These residues were Ser-74 of chain *C*1, Asn-153 of chain *R*1, Arg-54 of chain *C*6, and Gln-80, Lys-143, and Asn-153 of chain *R*6 (two examples are illustrated in Fig. 4). The strict criterion for alternate conformers delineated here does not eliminate the alternate positions described by Kim et al.[28] but places their conclusions at a lower level of reliability.

The next criteria demanded that the side chain angles conform with favorable values[57] of $\chi^1$ and $\chi^2$

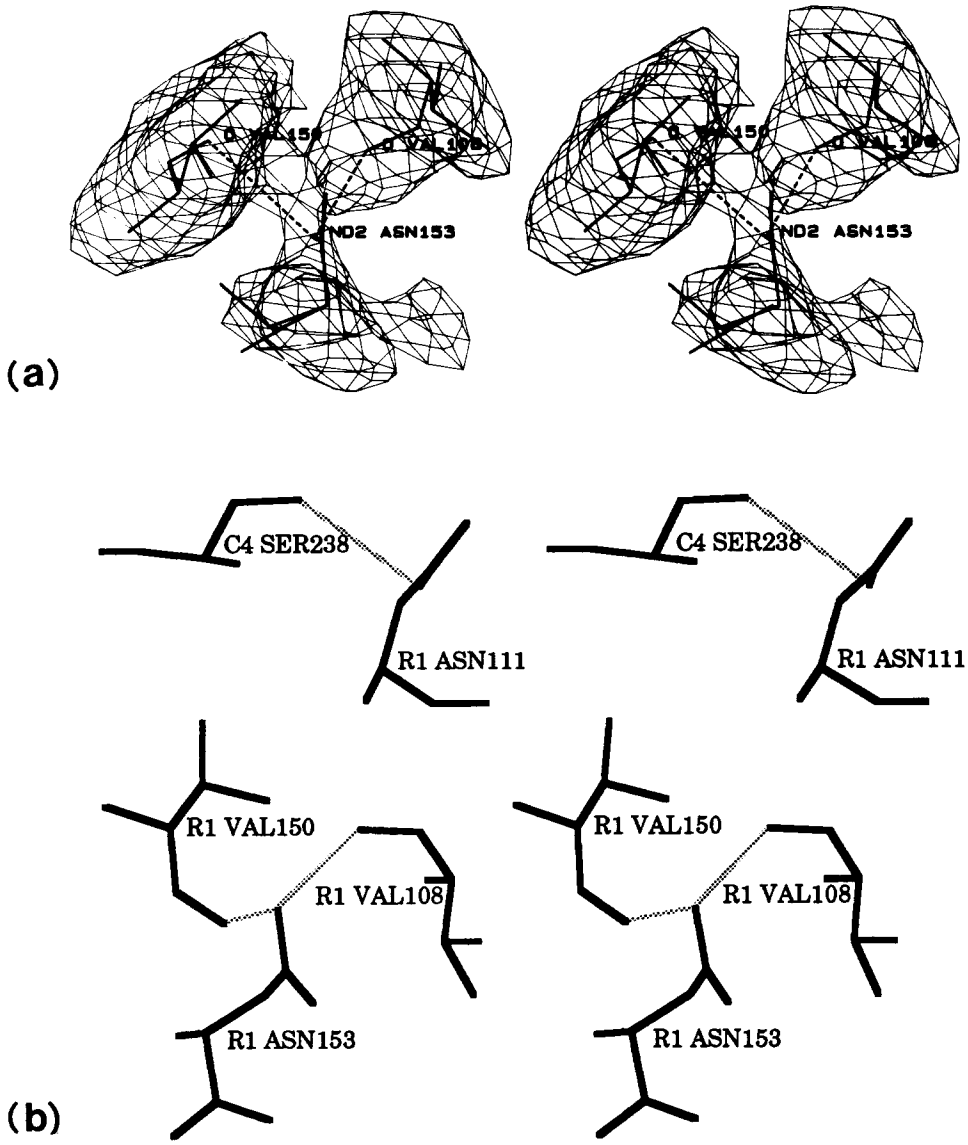


Fig. 5. **(a)** $(|F_o| - |F_c|)e^{i\alpha_{calc}}$ omit map which lacks $|F_c|$s from *R*1 Asn-153, Val-150, and Val-108. The contour level was 2.3σ. **(b)** Stick stereodiagram of residues which are hypothesized to form the mechanism of T state destabilization in the pAR5 mutant of ATCase.

and that the number of interactions the side chains form with nearby residues be similar. The orientation assumed by *C*1 Ser-74 subsequent to simulated annealing permitted an interaction between $O_{74}{}^{\gamma}$ and the main chain NH of *c*Asp-75 [3.1 Å($O_{74}{}^{\gamma}$, $N_{75}$)].[‖] Its $\chi^1$ was −164°, consistent with the finding that 28% of the 285 serine residues surveyed in 19 high resolution protein crystal structures (2.5 Å resolution or better) were found to be in the *trans* ($\chi^1$ = 180°) conformation.[57] In the other potential conformation of *C*1 Ser-74 $O_{74}{}^{\gamma}$ would have no polar contacts with other residues and would be assigned a $\chi^1$ of 9°, placing the hydroxyl directly above the amide NH. This conformation would lead to unfavorable van der Waals energies, and this potential conformer was therefore deemed unlikely.

The two potential conformers of *R*1 Asn-153 were in significantly different chemical environments. In its refined position, *R*1 Asn-153 lacked significant stabilizing interactions with neighboring residues. In fact, one of the carboxy-terminal oxygen atoms participated in electrostatically repulsive interactions with the main chain carbonyl oxygens of *R*1 Val-108 (3.4 Å) and *R*1 Val-150 (3.3 Å). When $\phi(C_{152},N_{153},C_{153}{}^{\alpha},C_{153})$ was rotated such that the

[‖]The convention employed in naming all amino acid constituents throughout this text is from the IUPAC-IUB Commission on Biochemical Nomenclature.[60]

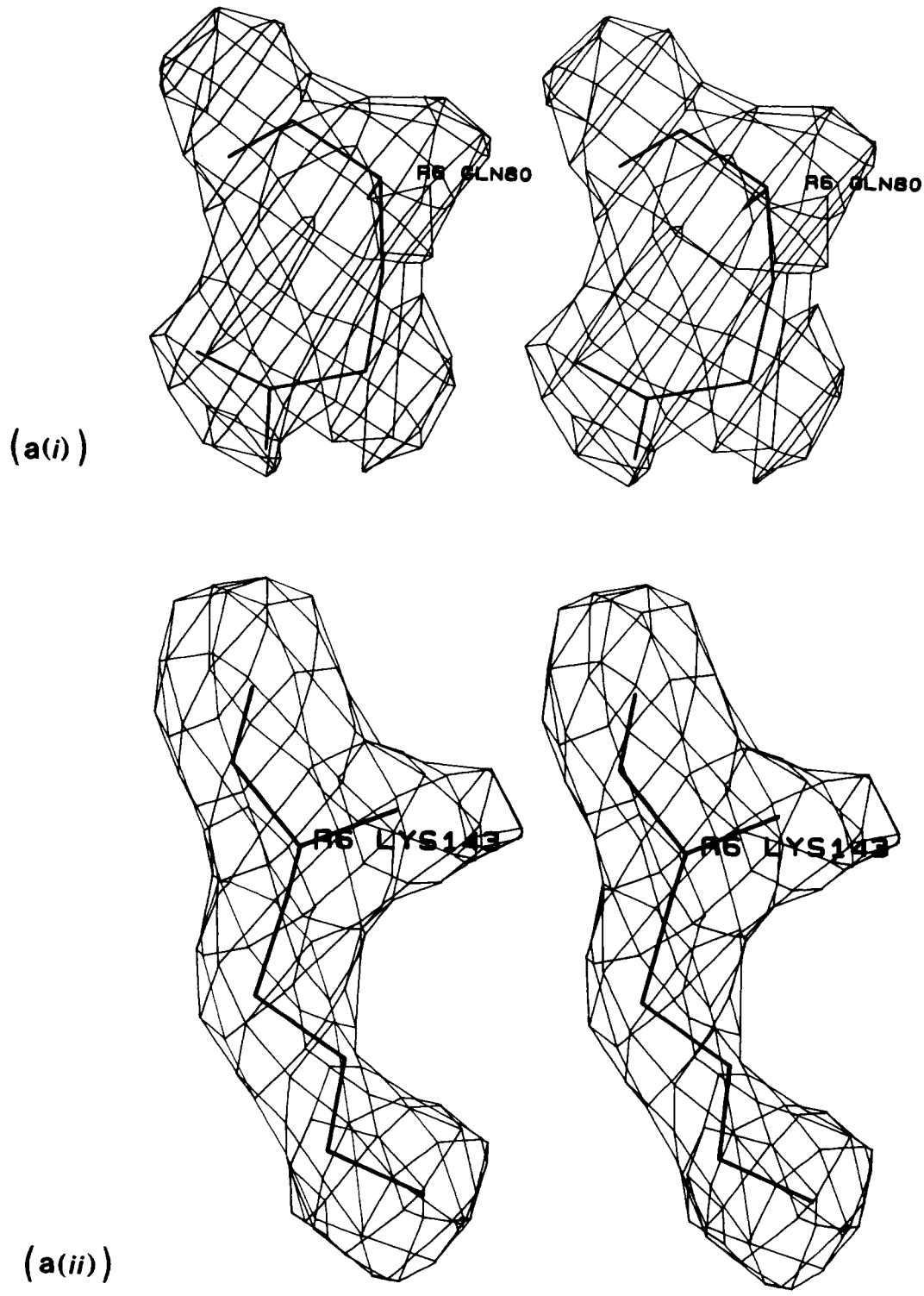


(a(*i*))

(a(*ii*))

Fig. 6. See next page for legend.

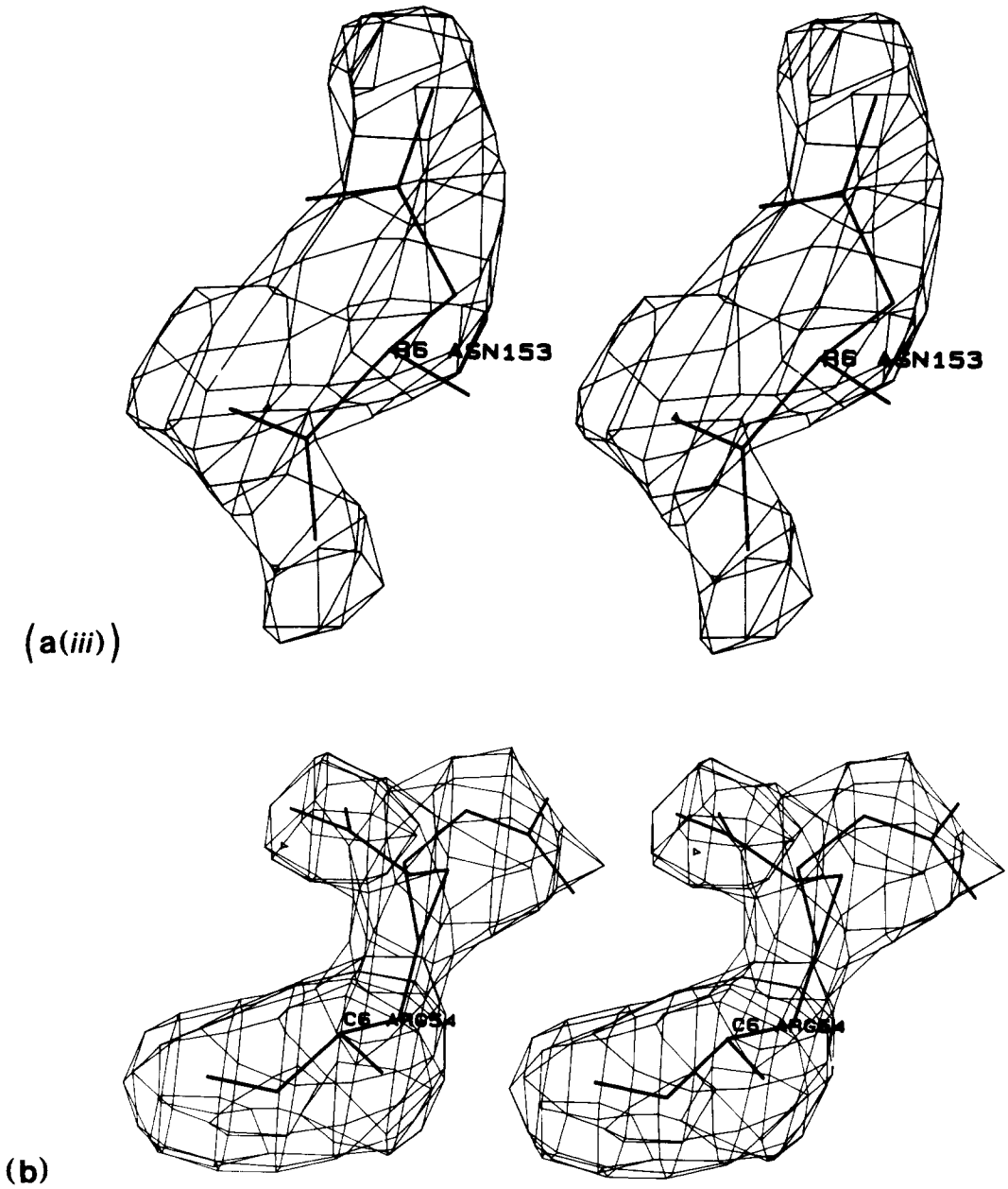


Fig. 6. **(a)** Omit maps with coefficients $(|F_o| - |F_c|)e^{i\alpha_{calc}}$ and lacking $|F_c|$s for Gln-80 (*i*), Lys-143 (*ii*), and Asn-153 ((*iii*); all of chain *R*6) — each indicating one preferred conformation for these residues when contoured at 2.0σ, 2.5σ, and 2.3σ, respectively. **(b)** Analogous omit map calculated for Arg-54 of chain *C*6. The contour level was 2.0σ. In both **(a)** and **(b)** the amino acids are drawn as stereo pairs.

side chain and carboxy-terminus of *R*1 Asn-153 were interchanged $N_{153}{}^{\delta 2}$ and the main chain carbonyl oxygens of *R*1 Val-108 and *R*1 Val-150 engaged in a hydrogen bonded network. The density in the $(2|F_o| - |F_c|)e^{i\alpha_{calc}}$ map favored this assignment and the calculation of an $(|F_o| - |F_c|)e^{i\alpha_{calc}}$ omit map** in which *R*1 Val-108, *R*1 Val-150, and *R*1 Asn-153 were omitted from the structure factor calculations also indicated that this position was preferred for *R*1 Asn-153 (Fig. 5a). The remaining four residues in potential alternate conformations satisfied the chemical criteria for alternate conformers.

**Omit maps are indispensable in locating errors in tentative models of X-ray crystal structures.[61–63] Consequently, they have been used extensively throughout this report.

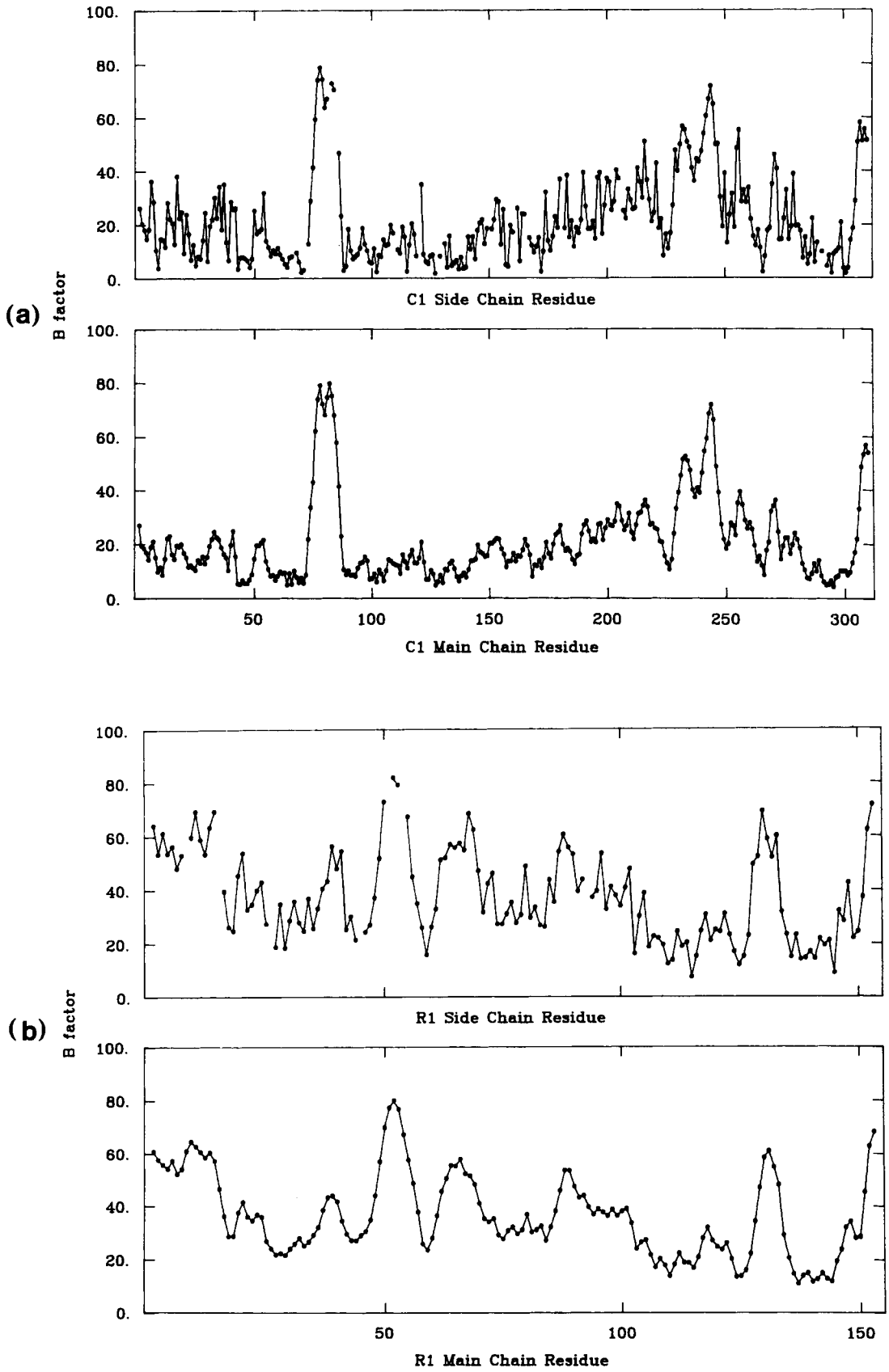


Fig. 7. See next page for legend.

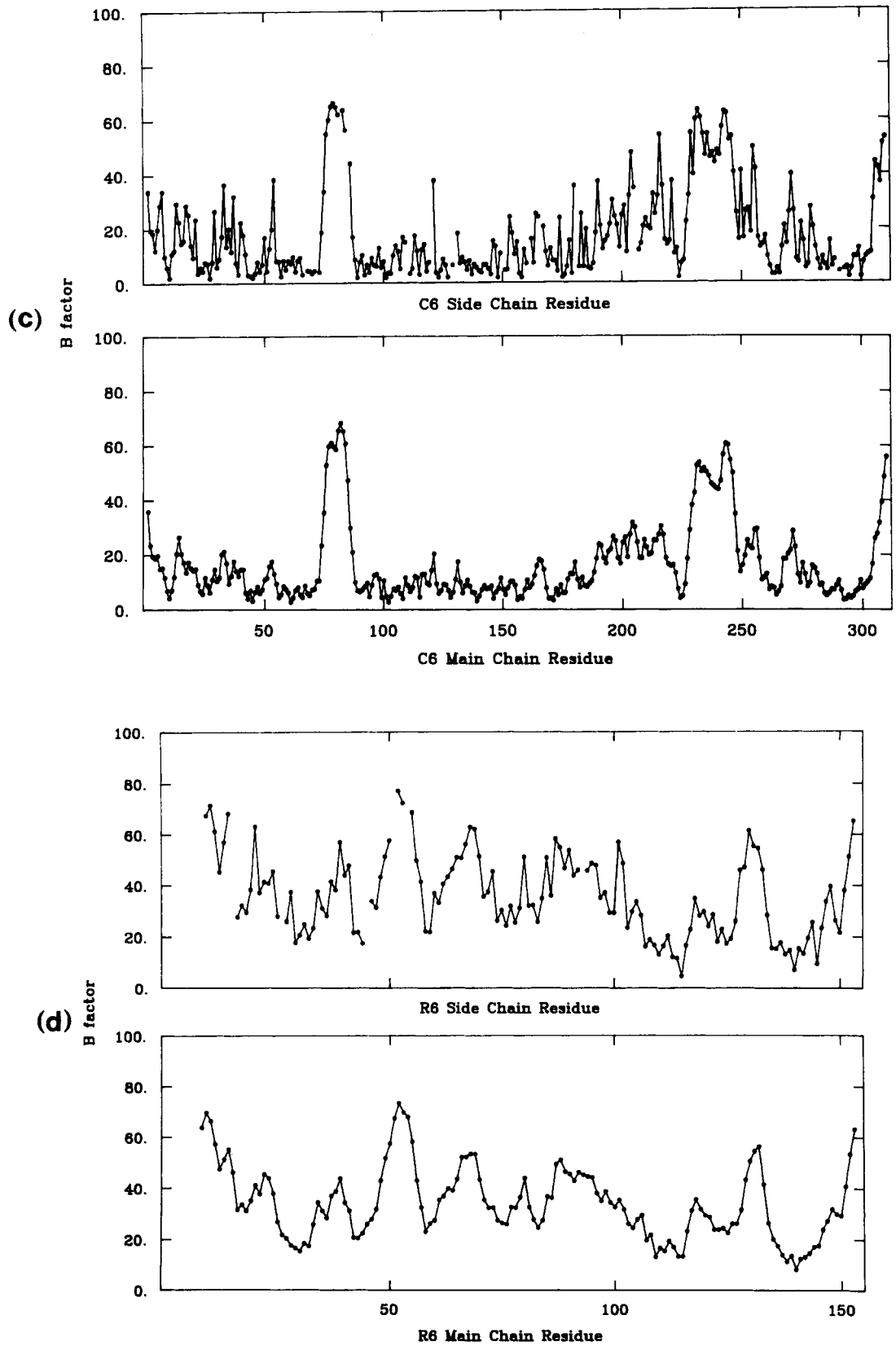


Fig. 7. Average *B* factor (Å$^2$) as a function of residue number for the side chain and main chain atoms of all of the residues in the asymmetric unit ((a)–(d)) of CTP-ligated T state ATCase. All glycines as well as the side chain of *r*Gln-8 have been omitted from the side chain plots, leading to the observed discontinuities. The average *B* factor for all nonhydrogen atoms in the structure (excluding solvent and the *R*6 residues Met-1—Leu-7) was 25.7 Å$^2$.

Omit maps with coefficients $(|F_o| - |F_c|)e^{i\alpha_{calc}}$ were generated for which *C*6 Arg-54, *R*6 Gln-80, *R*6 Lys-143, and *R*6 Asn-153 were omitted from the structure factor calculations. The omit maps indicated unequivocal positions for *R*6 Gln-80 and *R*6 Lys-143 [Fig. 6a(*i* and *ii*)]. Less impressive, though also apparently restricted to one position based on omit map density, was *R*6 Asn-153 [Fig. 6a(*iii*)]. The only residue which fulfilled the aforementioned criteria for designation as a true multiple conformer was *C*6 Arg-54. Its two potential conformations are depicted in Figure 6b.

Interestingly, the interaction reported between *R*1 Arg-130 and the β-phosphate CTP oxygen of a neighboring ATCase molecule in the crystal via a molecule of solvent[28] is absent in this crystal form of CTP-ligated **T** state ATCase, though a guanidinium nitrogen of *R*1 Arg-130 is situated 4.6 Å from a neighboring CTP α-phosphate oxygen (4.6 Å ($N_{130}{}^{\eta 2}$,$O_{999}{}^{\alpha 2}$); see the footnote to Table VI for the nomenclature used to describe CTP constituents). In its place are contacts between the side chains of *R*1 Arg-130 and *r*Glu-90 of a neighboring molecule in the crystal [2.9 Å($N_{130}{}^{\eta 2}$,$O_{90}{}^{\epsilon 2}$); 3.3 Å($N_{130}{}^{\eta 1}$, $O_{90}{}^{\epsilon 2}$)]. The interaction between these residues has recently been reported in the structure refinement of the **T** state of ATCase ligated with effectors.[27] In chain *R*6 the guanidinium $C_{130}{}^{\zeta}$ remains 20 Å from the nearest phosphate on a neighboring CTP molecule and 24 Å from the neighboring $C_{90}{}^{\delta}$ in the crystal. Though it is possible that these asymmetric interactions of *r*Arg-130 are biochemically significant conformations of the molecule which are selected by crystallization, it is more likely that the interactions are a consequence of packing forces in the crystal. The differences between the structure reported here and the structure described by Kim et al.[28] are probably due to the more complete and higher resolution data provided in the structure which forms the basis of this report and due to the uniformly poor electron density associated with the *r*130s loops in all crystal structures of ATCase.[27]

In Figure 7 the average *B* factor[††] is plotted for all of the side and main chain atoms of residues in the asymmetric unit. The values reported here are qualitatively and quantitatively similar to those determined in other recent X-ray crystal structure studies on the CTP-ligated,[28] ATP-ligated,[27] and unligated[26,27] forms of ATCase. Since *B* factors are determined empirically, they are the repository of errors resulting from the incorrect scaling of data, absorption effects, incorrect atomic scattering curves, and disorder.[64] Regions of spuriously high *B* factors in the structure which forms the basis of this report correspond to those regions recently identified when the refined **T** state structures of the ATP, CTP, and unligated forms of ATCase were compared.[27] In addition, very high temperature factors ($\geq 2.0B_{mean}$) are associated with residues 66–69 of both regulatory chains in the asymmetric unit. The average atomic *B* factors for chains *C*1, *R*1, *C*6, and *R*6 were 22.0, 37.6, 17.8, and 35.8 Å$^2$, respectively. As in an earlier study[27] the upper catalytic chain *C*1 has a slightly higher average *B* factor (approx. 4 Å$^2$) than its noncrystallographically related mate *C*6. This difference, though of a smaller magnitude (approx. 1 Å$^2$) when the *B* factors associated with *R*6 residues 1–7 are included, is conserved in the noncrystallographically related regulatory chains.

One of the cardinal goals of this study of the CTP-ligated form of ATCase as well as the goal of ongoing work on the various functional behaviors of the enzyme involves the determination and interpretation of conformational changes which accompany ligand binding. In this study, the effects of ligand binding are subtle and often occur in regions of protein that are disordered. Since the method of Luzzati[65] is not always effective in determining the expected errors in the coordinates of protein structures,[66] a different approach which has been employed previously[67] was adopted. From the simulated annealing refinements, there were eight structures which agreed almost equally well with the diffraction data and which had similar stereochemical quality (Table II). These structures were used to estimate the *minimal* uncertainty in individual atomic positions.

The ensemble of coordinates from simulated annealing refinement (Fig. 2) was used to determine mean atomic positions for all nonhydrogen atoms in the asymmetric unit. The rms deviation of each atomic position in the CTP-ligated structure was calculated using the eight refined structures and the mean structure. These rms values are shown in Figure 8 as a function of residue number for the main chain and side chain atoms and in Table IV as a function of polypeptide domain.

The results of this method of estimating the uncertainty in atomic positions are rms errors which are slightly smaller than the estimated errors for a previously refined CTP-ligated **T** state ATCase structure[28] as determined by a Luzzati plot.[65] However, as the data in Figure 8 indicate, the uncertainties in individual main chain or side chain atomic positions vary significantly from the rms value for the associated polypeptide chain and domain. These estimates of the individual coordinate error as well as the interdomain and intradomain variability have been used in the analysis of this structure and should be useful in analyses of other isomorphous complexes of ATCase.

[††]The average temperature factor for a residue was defined as the arithmetic mean of all the temperature factors associated with its nonhydrogen constituent atoms. All average *B* factors for the chains of ATCase cited in the text excluded all solvent, all hydrogen atoms, both molecules of CTP, and residues 1–7 of *R*6 from the calculations. The overall average *B* factor reported for the structure included temperature factors associated with CTP.

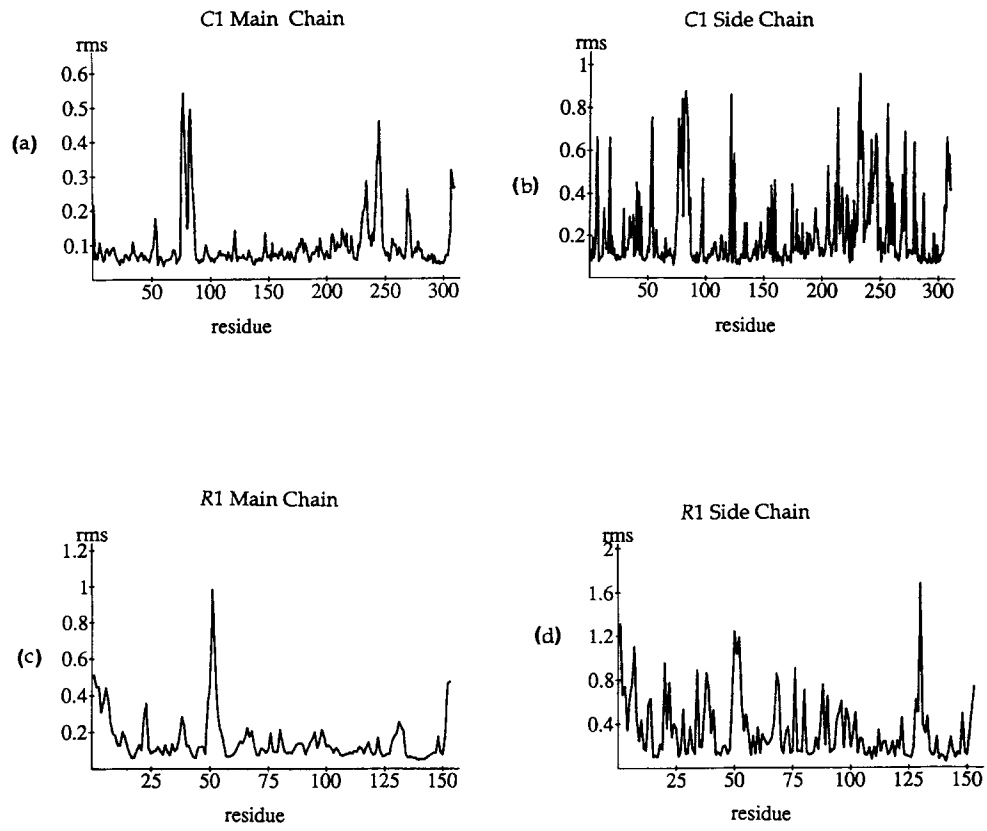


Fig. 8. The rms deviations (Å) of the eight molecular dynamics refined structures from the average structure for the *C*1 ((a),(b)) and *R*1 ((c),(d)) polypeptide chains as a function of residue number. The results for the noncrystallographically related chains *C*6 and *R*6 are qualitatively similar.

**TABLE IV. Average rms Errors (Å)* by Domain in Multiple Refinements of CTP-Ligated T State ATCase†**

| | *C*1 | | *C*6 | |
|---|---|---|---|---|
| | Main chain‡ | Side chain | Main chain | Side chain |
| Overall | 0.10 | 0.21 | 0.09 | 0.21 |
| CP§ (*c*1–140; *c*290–310) | 0.10 | 0.22 | 0.09 | 0.21 |
| asp (*c*141–289) | 0.09 | 0.19 | 0.09 | 0.21 |
| | *R*1 | | *R*6 | |
| Overall | 0.15 | 0.33 | 0.18 | 0.35 |
| all (*r*1–99) | 0.17 | 0.37 | 0.20 | 0.40 |
| zn (*r*100–153) | 0.12 | 0.25 | 0.13 | 0.27 |

$$*\text{atomic rms error} = \sqrt{\frac{\sum_{r=1}^{8} (X_r - X_{\text{mean}})^2}{(N = 8)}}$$

†The values reported for the domains are the arithmetic mean of the individual atomic rms errors for the constituents of the domain. The numbers in parentheses following the domain designations refer to the amino acid constituents of the domain utilized in the calculations.

‡($N_i$,$C_i^{\alpha}$,$C_i$) were used in the calculation of main chain rms errors.

§CP, carbamoyl phosphate.

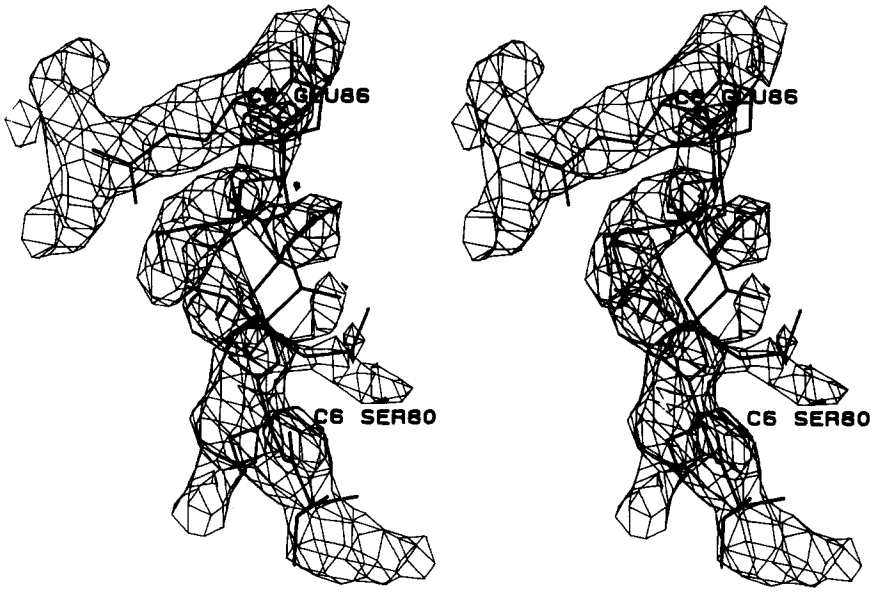


Fig. 9. $(|F_o| - |F_c|)e^{i\alpha_{calc}}$ map in which the $|F_c|$ contribution from *C*6 74—86 was omitted. The contour level was set to 2.0σ. *C*6 Thr-79—Glu-86 are depicted in the stereodiagram.

Though density associated with the *c*80s loop of **T** state CTP-bound ATCase has been notoriously poor,[25,28] the repositioning of *C*1 76–85 and *C*6 76–86 yields a superior fit with the weak electron density in an $(|F_o| - |F_c|)e^{i\alpha_{calc}}$ omit map in the region of *C*1 and *C*6 80–85 (Fig. 9). In Figure 10 the differences in the traces of the backbone peptide atoms ($N_i$, $C_i^\alpha$, $C_i$, and $O_i$) are illustrated. However, the persistently high *B* factors and high rms errors associated with the *c*80s loop (Figs. 7 and 8) and the results of a least squares superposition of all of the main chain atoms of the two catalytic chains of the asymmetric unit ($rms_{\text{all backbone of } C \text{ chain}}$ = 0.7 Å; $rms_{\text{backbone of 76–86}}$ = 2.1 Å)[‡‡] indicates that while the retrace of the loop (Figs. 9 and 10) afforded an opportunity to utilize the larger data set available from this refinement of the CTP-ligated **T** state ATCase structure, it is unclear whether the retrace has objectively improved this portion of the structure as indicated by the persistently high thermal parameters, the high rms errors, and the apparent generation of another violation of molecular 2-fold symmetry. The inability to improve the position of the *c*80s loop as measured by objective criteria may simply be a consequence of the inherent flexibility of this loop in the **T** state of the enzyme.

The significance of the *c*80s loop in ATCase lies in its contribution to catalytic events in the active site of a neighboring catalytic chain within the same trimer. The suggestion that active sites on ATCase are shared between adjacent catalytic chains within a given catalytic trimer $c_3$ was first made on the basis of the X-ray crystal structures of the unligated and CTP-complexed **T** forms of ATCase.[20] *c*Lys-83 and *c*Lys-84 are currently believed to provide a recognition and guidance mechanism for the binding of L-aspartate and carbamoyl phosphate in the active site.[26,29] *c*Ser-80 is important for communication between the catalytic chains, though it does not perform a prominent role in catalysis.[69] The link between *C*1 Arg-54 and *C*2 Glu-86[25,28] is a prominent salt link in the *C*1–*C*2–*C*3 interface, though the catalytic chains contributing to the interface region are tethered together by a multitude of amino acid side chain polar contacts. The side chain of *C*1 Arg-54, in addition to interacting with the side chain of *C*2 Glu-86, is oriented such that it is at the outer limit of forming a charge-polar interaction with the main chain carbonyl oxygen of *C*2 Asp-90. This interaction is not formed by *C*6 Arg-54. Kim et al.[28] were the first to document the involvement of *C*2 Tyr-98 in the *C*1–*C*2–*C*3 interface. In the structure which forms the substance of this report, the side chain of *C*2 Tyr-98 interacts with the carbonyl oxygen of *C*1 Arg-54 (Table V). This interaction is absent in chain *C*6. In turn, the carbonyl oxygen of *C*2 Tyr-98 interacts with the side chain of *C*1 Arg-65, which interacts with the side chain of *C*2 Asp-100 and the carbonyl oxygen of *C*2 His-41 (Fig. 11). Presumably, this network of interactions serves to tether the trimers of the CTP-ligated **T** state to-

[‡‡]This superposition, as with all main chain superpositions throughout this report, utilized the least squares method of Kabsch[68] as it is incorporated in X-PLOR[51] to minimize the rms deviations of $(N_i, C_i^\alpha, C_i)$.

All distances between constituents of different structures reported in the text were calculated subsequent to least squares superposition[51,68] of the relevant structures.

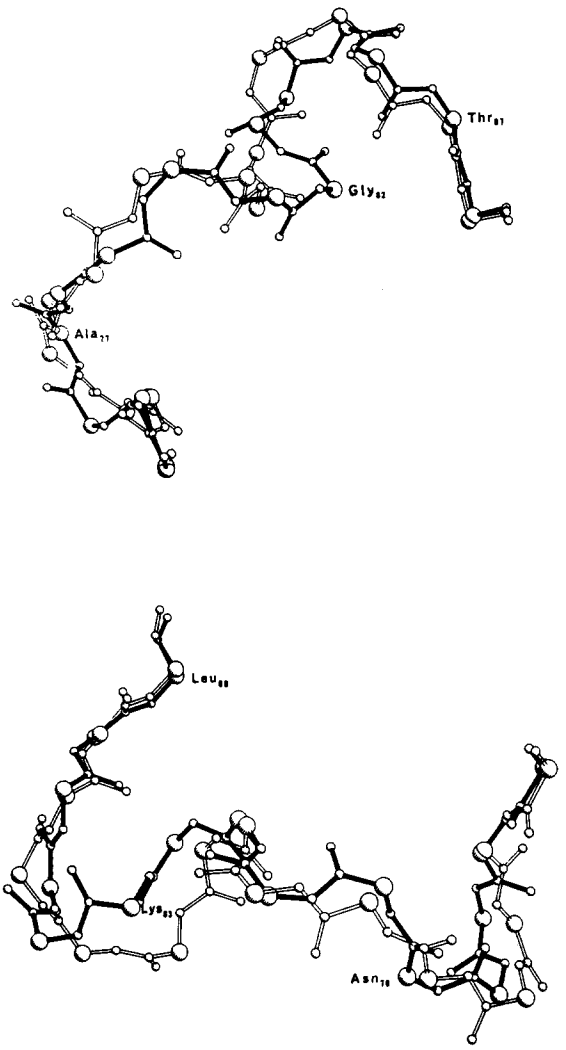


Fig. 10. Constituent main chain atoms of the *c*80s loop before[28] (light) and after (dark) the loop was refitted. The diagram on the top of the figure compares *C*1 74—88, while the diagram on the bottom of the figure compares the analogous residues of *C*6. The $C^{\alpha}$ were enlarged relative to the other main chain atoms for clarity. Only the $C^{\alpha}$ of the CTP-ligated ATCase structure which forms the basis of this report are labeled in the diagrams.

gether appropriately such that residues required for catalysis (e.g., *c*Arg-54) are oriented correctly in the active site. Recent mutagenesis work on active site residues in the catalytic chains of ATCase[70] has more narrowly defined a role for *c*Arg-54 in the catalytic mechanism of ATCase. The residue is essential for catalysis and less important in the binding of carbamoyl phosphate as demonstrated by the *c*Arg-54 → Ala mutant's 17,000-fold reduction in maximal activity and 13-fold reduction in affinity for carbamoyl phosphate. Mutagenesis work on the residues outlined above may elucidate their potential role in securing the proper orientation for *c*Arg-54 in the CTP-ligated **T** state structure and may lead to an appreciation of how these interactions are utilized in catalysis and in the transition from the **T** → **R** state.

## The Binding of CTP

Previous reports on the crystal structure of CTP-ligated **T** state aspartate transcarbamoylase identified the γ-phosphate of CTP in the carbamoyl phosphate domain of the active site.[13,41] Inspection of an $(|F_o| - |F_c|)e^{i\alpha_{calc}}$ omit map, at contour levels as low as 1.5σ, did not yield evidence that CTP was present in this site. This contrasts with the unambiguous presence of both molecules of CTP in the allosteric effector domains of the *R*1 and *R*6 chains of the asymmetric unit. Stereoviews of the *R*1 and *R*6 CTPs are provided in Figures 12 and 13, respectively. At an acceptable threshold (2σ), the electron density in the region of the atoms bridging the ribose and α-phosphate ($C^{5'}$ and $O^{5'}$) of *R*1 and *R*6 CTP is absent. The contour level had to be lowered to 1.5σ and 0.6σ in an $(|F_o| - |F_c|)e^{i\alpha_{calc}}$ omit map for the discontinuities in the electron density associated with the *R*1 and *R*6 CTPs to be eliminated, respectively. There are three chemical, though (due to the complete absence of experimental evidence) unlikely, explanations for this absence of electron density. These unsubstantiated chemical possibilities include a slow phosphatase activity associated with the allosteric site (there are several amino acid side chains near the allosteric binding site which are capable of performing a catalytic role, e.g., *r*Ser-50, *r*Thr-82, or *r*Asp-19), the nonenzymatic hydrolysis of CTP, or cytidine and triphosphate impurities of CTP. However, a preliminary **R** state ATCase crystal structure of the enzyme ligated with PAM/malonate and CTP + UTP at pH 7.0 and at 2.2 Å resolution[71] demonstrates continuous electron density around the atoms bridging the nucleoside and triphosphate groups in the *R*1 site at an acceptable contour level of 2.0σ. Furthermore, if the nucleotides existed as their constituent nucleosides and triphosphates in the allosteric binding site crystal structures of the enzyme with nucleotides, which are sensitive to and demonstrate variation in binding between the nucleotides in the different regulatory chains, should demonstrate variations in the occupancies between the nucleoside and the triphosphate within any one site. This has never been described. Therefore, it appears that the systematic absence of electron density is probably a consequence of the flexibility of this portion of the molecule which links the cytidine and triphosphate moieties, a consequence of the dominant atomic scattering of the α-phosphate, and/or a result of Fourier series termination errors.

The cytosine base of both molecules of CTP is oriented *anti* with respect to the ribose ring, as has been found in nearly all X-ray structures of nucleic acids and pyrimidine nucleotides.[72] The torsion angle $\chi_{CN}$, defined as the angle formed by the plane of

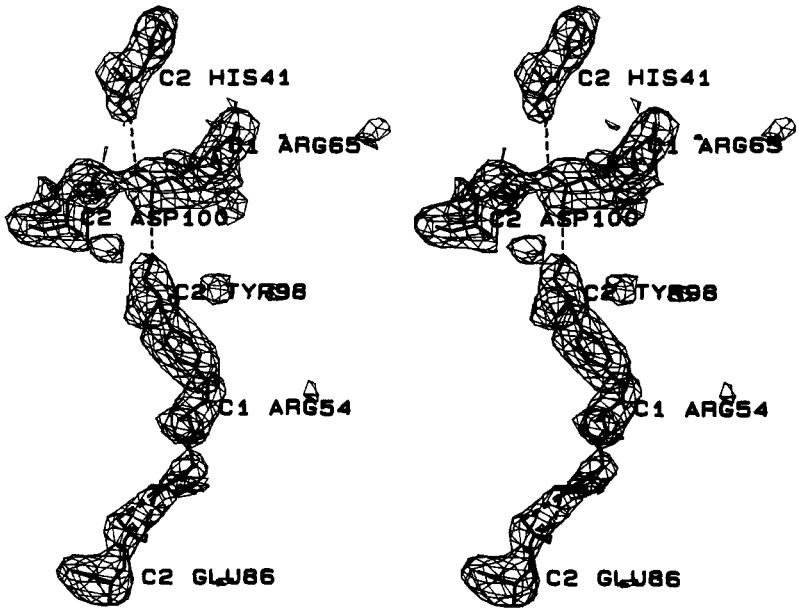


Fig. 11. The amino acid side chains contributing to the correct orientation of the active site residue *c*Arg-54. The map in the figure was calculated with the coefficients $(|F_o| - |F_c|)e^{i\alpha_{calc}}$ and without $|F_c|$s from *C*1 Arg-54, *C*2 Glu-86, *C*2 Tyr-98, *C*1 Arg-65, *C*2 Asp-100, and *C*2 His-41. The map for this stereodiagram was contoured at 2.5σ.

**TABLE V. Polar Contacts Relevant to the Arginine 54/Glutamate 86 Network in the *C*1–*C*2–*C*3 Interface Region of CTP-Ligated T State Aspartate Transcarbamoylase***

| Atom pair | Distance (Å) (chain *C*1) | Distance (Å) (chain *C*6) |
|---|---|---|
| Arg $N_{54}{}^{\eta 1}$–C2 Glu $O_{86}{}^{\epsilon 1}$ | 2.8 | 2.7† |
| Arg $N_{54}{}^{\eta 1}$–C2 Glu $O_{86}{}^{\epsilon 2}$ | 2.9 | 3.3† |
| Arg $N_{54}{}^{\eta 1}$/C6 Arg $N_{54}{}^{\eta 2}$–*C*2/*C*5 Asp $O_{90}$ | 3.5 | 6.0† |
| Arg $N_{54}{}^{\eta 2}$–*C*2 Glu $O_{86}{}^{\epsilon 1}$ | 3.3 | 3.5† |
| Arg $N_{54}{}^{\eta 2}$–*C*2 Glu $O_{86}{}^{\epsilon 2}$ | 3.1 | 2.5† |
| Arg $N_{54}{}^{\epsilon}$–*C*2 Glu $O_{86}{}^{\epsilon 1}$ | 4.6 | 3.2† |
| Arg $N_{54}{}^{\epsilon}$–*C*2 Glu $O_{86}{}^{\epsilon 2}$ | 4.9 | 3.0† |
| Arg $O_{54}$–*C*2 Tyr $O_{98}{}^{\eta}$ | 3.2 | 3.9 |
| *C*2 Tyr $O_{98}$–Arg $N_{65}{}^{\eta 2}$ | 3.2 | 2.9 |
| Arg $N_{65}{}^{\eta 1}$–*C*2 Asp $O_{100}{}^{\delta 1}$ | 3.2 | 3.3 |
| Arg $N_{65}{}^{\eta 1}$–*C*2 Asp $O_{100}{}^{\delta 2}$ | 2.7 | 2.8 |
| Arg $N_{65}{}^{\eta 1}$–*C*2 His $O_{41}$ | 3.5 | 3.4 |

*All residues not given a chain designation are constituents of *C*1. Atoms which differed among the two chains *C*1 and *C*6 in the interaction distance calculations are indicated and separated by a slash ("/").

†All distances cited for the side chain of *C*6 Arg-54 consistently employ one of the two conformers of this residue.

$O^{1'}$, $C^{1'}$, and $N^1$ relative to the plane formed by $C^{1'}$, $N^1$, and $C^6$, was 33° for *R*1 CTP and 40° for *R*6 CTP. These values are very similar to the reported $\chi_{CN}$ of 34.2° observed in the zinc complex with the monomethyl 5′-phosphate ester of CMP.[73] The $C^{2'}$-*endo* and $C^{3'}$-*endo* conformations of the furanose ring of monomeric ribonucleotides are observed with nearly equal frequency in X-ray crystal diffraction experiments and nuclear magnetic resonance studies.[72] For the CTP molecules in the *R*1 and *R*6 allosteric sites, the orientation of the atoms in the ribose ring is consistent with either the $C^{2'}$-*endo* or the $C^{3'}$-*endo* conformation. At this resolution (2.5 Å) a crystallographic distinction between these possibilities cannot be made.

The interactions between T state ATCase and *R*1 and *R*6 CTP are summarized in Table VI. The 4-amino group of *R*1 and *R*6 CTP acts as a hydrogen bond donor to the main chain carbonyl oxygens of *r*Tyr-89 and *r*Ile-12, while the 4-amino group of *R*6 CTP forms a potential contact with the main chain NH of *R*6 Ile-12. CTP $N^3$ interacts with the main chain NH of *r*Ile-12. The cytosine 2-keto group from *R*1 CTP is involved in an interaction with the amino group of *R*1 Lys-60. The 2-keto group of *R*6 CTP is too far from *R*6 Lys-60 to form a similar interaction. The amino group of *R*1 Lys-60 and the carbonyl oxygen of *R*1 Val-9 are capable of interacting with the 2′-hydroxyl of *R*1 CTP; these interactions, in addition to the interaction between the side chain of *R*1 Lys-60 and the 2-keto group of *R*1 CTP, are not conserved in the analogous *R*6 chain site. One of the carboxylate oxygens of *R*6 Asp-19 forms a charge-polar interaction with the 3′-hydroxyl of *R*6 CTP although the analogous interaction is absent in the *R*1 site. The amino group of *R*1 Lys-94 interacts with an α-phosphate oxygen of *R*1 CTP, while *R*6 Lys-94 interacts with two γ-phosphate oxygens of *R*6 CTP. The hydroxyl of *R*6 Thr-82 interacts with a γ-phosphate oxygen of *R*6 CTP while $N^{\epsilon 2}$ of *R*1 His-

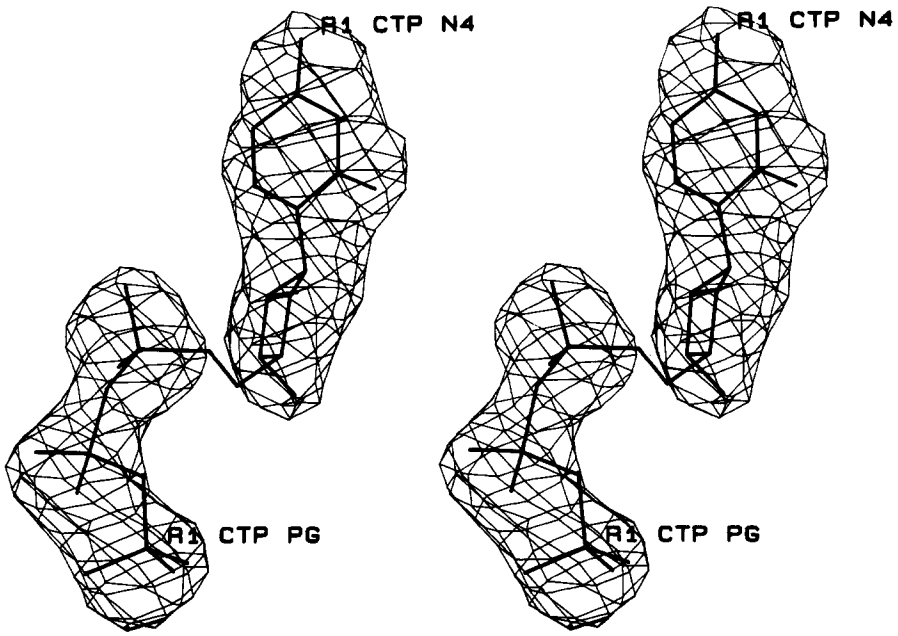


Fig. 12. Stereoview of *R*1 CTP. The map density is from an $(|F_o| - |F_c|)e^{i\alpha_{calc}}$ omit map in which the $|F_c|$s from both molecules of CTP were excluded from the calculations. The map was contoured at 2.5$\sigma$. Hydrogen atoms have been excluded from the figure.

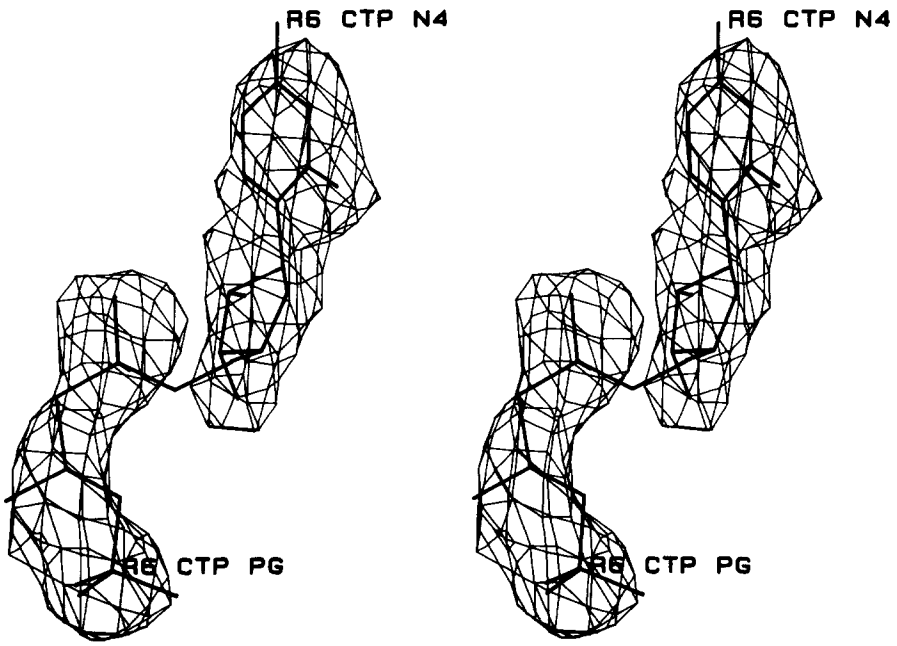


Fig. 13. Stereoview of *R*6 CTP. The $(|F_o| - |F_c|)e^{i\alpha_{calc}}$ omit map was contoured at 2.5$\sigma$. As in Figure 12, all hydrogen atoms have been omitted.

**TABLE VI. Contacts Between CTP and T State Aspartate Transcarbamoylase***

| Atom pair† | Distance *R*1/*R*6 (Å) |
|---|---|
| Tyr $O_{89}$–CTP 4-amino | 3.4/3.0 |
| Ile $O_{12}$—CTP 4-amino | 3.0/2.8 |
| Ile $N_{12}$—CTP 4-amino | 3.9/3.5 |
| Ile $N_{12}$—CTP $N^3$ | 3.2/2.9 |
| Lys $N_{60}^{\zeta}$—CTP 2-keto | 3.1/5.1 |
| Lys $N_{60}^{\zeta}$—CTP 2′-OH | 3.3/4.9 |
| Val $O_9$—CTP 2′-OH | 3.3/6.5 |
| Asp $O_{19}^{\delta 2}$—CTP 3′-OH | 4.1/2.9 |
| Lys $N_{94}^{\zeta}$—$O_{999}^{\alpha 3}$ | 3.0/5.3 |
| $H_2O$–*R*1 $O_{999}^{\alpha 3}$/*R*6 $O_{999}^{\beta 3}$ | 4.8/3.4 |
| Lys $N_{94}^{\zeta}$—$O_{999}^{\gamma 2}$ | 4.0/2.8 |
| Lys $N_{94}^{\zeta}$—*R*1 $O_{999}^{\gamma 1}$/*R*6 $O_{999}^{\gamma 3}$ | 4.5/2.9 |
| Thr $O_{82}^{\gamma}$—*R*1 $O_{999}^{\gamma 2}$/*R*6 $O_{999}^{\gamma 3}$ | 4.1/3.2 |
| *R*1 His $N_{20}^{\epsilon 2}$/*R*6 His $N_{20}^{\delta 1}$—$O_{999}^{\gamma 3}$ | 2.8/7.3 |

*A subscripted residue number 999 refers to CTP, while the phosphate a particular CTP oxygen is bound to is indicated by a superscript. The labeling of triphosphate oxygens treats the atoms as if they formed a chain beginning at the α-phosphate and terminating on the γ-phosphate in a manner analogous to that described by the IUPAC-IUB Commission[60] for amino acids. All unlabeled atoms are from *R*1. Slashes are used to distinguish the atoms employed in the distance calculations if there were differences between the two CTP binding sites defined by the asymmetric unit.

†Since both pairs of α- and β-phosphate oxygens of CTP are unprotonated, the two oxygen atoms within each pair are indistinguishable. One of the terminal γ-phosphate oxygens has a $pK_a > 5.8$ (the pH of this study), and at its location on the solvent exposed face of the allosteric site it should be distinguishable from the other two γ-phosphate oxygens. However, given the limited number of contacts between CTP and ATCase and the limited resolution of this work, discerning which oxygen is protonated is not possible. Consequently, all γ-phosphate oxygens are treated as if they are equivalent.

20 interacts with one of the γ-phosphate oxygens of *R*1 CTP. This is the first report of the interaction between *r*Thr-82 and CTP, and the application of site-directed mutagenesis on *r*Thr-82 to establish the importance of this residue in the binding of nucleotide effectors is encouraged. Finally, *R*6 CTP interacts with a molecule of solvent—a β-phosphate oxygen accepts a hydrogen bond from a molecule of solvent. This water molecule makes no other contacts which can be traced back to the enzyme.

## THE FIRST SEVEN RESIDUES OF THE REGULATORY CHAIN

This refinement of the CTP-ligated **T** state aspartate transcarbamoylase structure represents the first recent refinement of ATCase in either the **T** or **R** state[27,28,30,33] which possessed adequate electron density to assign positions to the first seven residues of the regulatory chains which have been implicated in the binding of nucleotides and, as a consequence, implicated in the heterotropic effects.[25,27,41,42]

Omit maps with coefficients $(|F_o| - |F_c|)e^{i\alpha_{calc}}$ were used to establish the validity of the positions that were assigned to the first seven residues of the regulatory chain of ATCase prior to simulated annealing. Diffuse map density at what was deemed the minimal acceptable contour level (2.0σ) led to the rejection of the tentative positions of the first seven residues of chain *R*6 (Fig. 14). Specifically, at this contour level acceptable electron density was associated only with the side chains of residues *r*His-3, *r*Asn-5, and *r*Leu-7, the three terminal side chain atoms of *r*Met-1, and the main chain atoms of *r*Thr-2, *r*Asn-5, and *r*Lys-6. Therefore, the coordinates of the first seven residues of chain *R*6 were removed from the final coordinate file.

When the $(|F_o| - |F_c|)e^{i\alpha_{calc}}$ omit map which excluded the $|F_c|$s from the first seven residues of chain *R*1 was contoured at 2.4σ only the main chain NH and $C^{\alpha}$ of *R*1 Thr-2, the main chain carbonyl oxygen of *R*1 Asn-5, and $C^{\delta 1}$ of *R*1 Leu-7 had no appreciable electron density (Fig. 15a). All other main chain atoms and the side chains of *R*1 Thr-2, *R*1 His-3, *R*1 Asp-4, *R*1 Asn-5, and *R*1 Lys-6 were easily traced in acceptable electron density at this contour level. The first seven residues of *R*1 are oriented in an extended conformation, and the (ϕ,ψ) torsion angles[59] for these residues are not consistent with any of the well-defined secondary structure motifs.[60] In Table VII the potential interactions among the first seven residues of chain *R*1 and with surrounding residues of ATCase are listed. The amino-terminus donates a hydrogen bond to the terminal hydroxyl of *R*1 Tyr-89 (Fig. 15b). The main chain carbonyl oxygen of *R*1 Thr-2 accepts a hydrogen bond from the amide NH of *R*1 Asp-4. The side chain hydroxyl of *R*1 Thr-2 interacts with the terminal amino of *r*Lys-129, the main chain carbonyl oxygen of *r*Asn-132, and the side chain amide oxygen of *r*Asn-132—all of a neighboring molecule in the crystal (i.e., an interhexamer contact). The imidazole $N^{\delta 1}$ of *R*1 His-3 forms a salt link with a carboxylate oxygen of *R*1 Glu-10 and forms hydrogen bonds with the side chain hydroxyl of *R*1 Thr-2 and the main chain carbonyl oxygen of *r*Asn-132 (an interhexamer contact). The imidazole $N^{\epsilon 2}$ of *R*1 His-3 donates a hydrogen bond to the main chain carbonyl oxygen of *r*Asp-133 (another interhexamer contact). The main chain carbonyl oxygen of *R*1 Asp-4 accepts a hydrogen bond from the amide NH of *R*1 Glu-10. The main chain carbonyl oxygen of *R*1 Asn-5 accepts a hydrogen bond from the main chain NH of *R*1 Val-9, while the side chain $O^{\delta 1}$ of *R*1 Asn-5 accepts a hydrogen bond from the main chain NH of *R*1 Leu-7. The side chain amide nitrogen of *R*1 Asn-5 interacts with the main chain carbonyl oxygen of *R*1 Gln-8. Interestingly, there are two interactions which span the molecular 2-fold axis near the amino-terminus of both regulatory chains. The main chain NH of *R*1 Asn-5 donates a hydrogen bond to the carbonyl oxygen of *R*6 Gln-8, while the main chain NH of *R*1

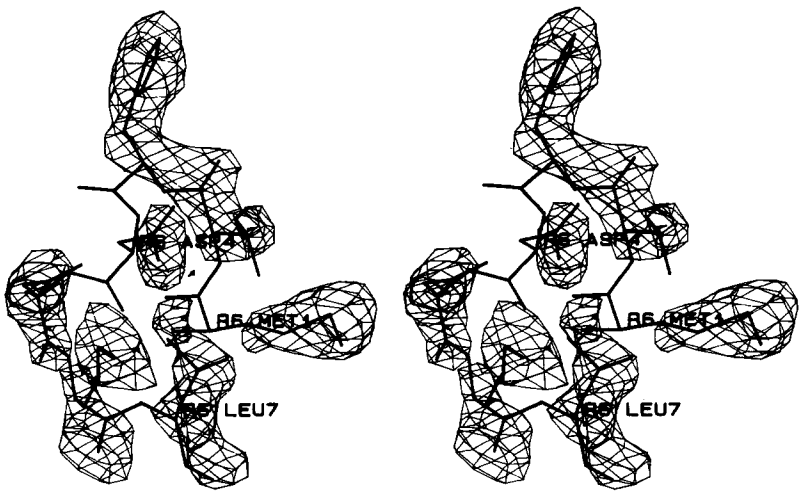


Fig. 14. Stereodiagram of the 7 amino-terminal residues of chain *R*6. The electron density map utilized coefficients of $(|F_o| - |F_c|)e^{i\alpha_{calc}}$ in which the $|F_c|$s from all atoms of the first 7 residues were omitted. The map was contoured at 2.4σ.

Lys-6 engages in a charge-polar interaction with a side chain oxygen of *R*6 Glu-10. Finally, the main chain carbonyl oxygen and the terminal $N^{\zeta}$ of *R*1 Lys-6 interact with the main chain NH of *R*1 Gln-8 and a carboxylate oxygen of *R*6 Glu-62, respectively.

The importance of the locations of the first seven residues may reside in their relationship to *R*1 Asp-87—*R*1 Val-91 (*r*80s loop). These residues shift away from the allosteric pocket upon binding of CTP to the enzyme and permit CTP to enter the allosteric binding site (average $\Delta C_{88-90}{}^{\alpha}$—1.4 Å). The movement of this *r*80s loop is restrained by a charge-polar interaction between the side chain of *R*1 Tyr-89 and the amino-terminus [2.5 Å($O_{89}{}^{\eta}$,$N_1$); Fig. 15b]. This is the first structural identification of the potential importance of both *r*Tyr-89 and the first seven residues of the regulatory chain in the mechanism of CTP binding to ATCase. A recent NMR study on 3-fluorotyrosine-labeled ATCase regulatory chains[74] showed that the addition of increasing amounts of ATP to the regulatory subunits of the enzyme resulted in a sharpening and a small (an average of 0.1 ppm for two samples) shift upfield in the spectrum of the unligated form of ATCase while CTP, in addition to sharpening the peak associated with native ATCase, caused the appearance of a second peak 0.4 ppm downfield. This result indicates that the presence of nucleoside triphosphates at the allosteric site on the enzyme perturbs the environment of tyrosine residues in the regulatory subunits. This result differs from an earlier NMR study[75] in which no significant perturbation of the $\gamma$-$^{13}$C-labeled tyrosine spectrum of ATCase regulatory subunits was observed upon complexation with ATP or CTP. The differences between these two NMR studies might be related to the location of their probes:[74] $^{19}$F was located *ortho* to the hydroxyl group on *r*Tyr-89, and $^{13}$C was directly opposed to the $C^{\zeta}$ which is adjacent to the hydroxyl group of the ring. Another potential explanation for these conflicting results may lie in the comparatively low signal-to-noise ratio of $\gamma$-$^{13}$C spectra of regulatory subunits of ATCase.[75] It is also possible that the polar nature of the probe used in $^{19}$F-NMR experiments might influence the conformation adopted by the tyrosine residue to which it is bound—despite similar responses to nucleotides, similar dissociation and exchange properties of the catalytic and regulatory subunits, and similar decreases in the sedimentation coefficient in the presence of PALA.[74]

The displacement of the *r*80s loop facilitates the accommodation of the cytosine base of CTP in the allosteric binding site. The addition of the coordinates of CTP to the unligated T state coordinate set[27] yielded a separation of 2.2 Å between the CTP 4-amino group and $C_{89}{}^{\alpha}$. In purines such as ATP this interaction between the base and the *r*80s loop should be more pronounced, and recent site-directed mutagenesis work by Kantrowitz and colleagues[76] shows that when *r*Tyr-89 is replaced by Ala the ATP activation of this ATCase mutant is enhanced. This result is possibly a consequence of the loss of the link between the side chain of *r*Tyr-89 and the amino-terminus which permits a more open nucleotide base subsite. An experiment which would further probe the importance of the relative mobility of the *r*80s loop would be the creation of site-directed mutants with glutamate or phenylalanine in place of *r*Tyr-89. In the absence of structural information detailing the location of the first seven residues of the regulatory chain of the unligated form of ATCase,

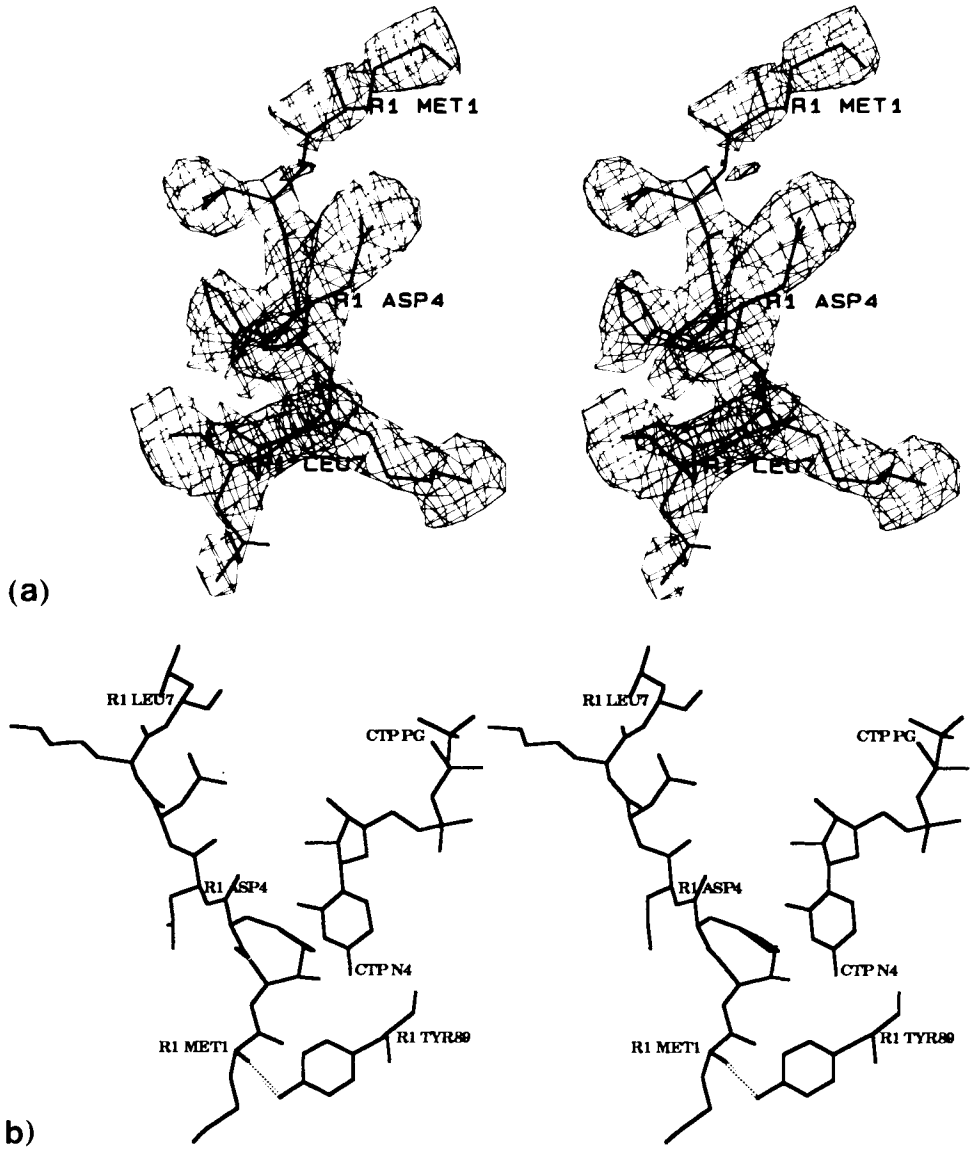


Fig. 15. **(a)** Stereoview of the analogous residues of chain *R*1. The density is from an $(|F_o| - |F_c|)e^{i\alpha_{calc}}$ omit map which was contoured at 2.4$\sigma$. **(b)** A stick drawing which illustrates the orientation and location of the first seven residues of chain *R*1. Note the charge-polar interaction between the side chain of *r*Tyr-89 and the amino-terminus (see text).

these mutants might provide more insight into the role of the charge-polar interaction between *R*1 Tyr-89 and the amino-terminus as the enzyme binds nucleotides.

### The pAR5 Mutant of ATCase

The pAR5 mutant of aspartate transcarbamoylase, in which the eight carboxy-terminal amino acid residues of the regulatory chains of wild-type ATCase are replaced with a new sequence of six residues, has been shown to lack substrate cooperativity and inhibition by CTP although the response to ATP is normal.[38] Though the mutant has been utilized to elucidate the homotropic and heterotropic functions of the native enzyme,[39,77] in this section emphasis is placed upon how the homotropic behavior of the mutant can be described in the context of the homotropic pathways already devised for the native enzyme and the structure which represents the basis of this report.

X-ray solution scattering studies and molecular mechanics simulations on the pAR5 mutant suggested that it adopts a conformation consistent with an intermediate between the **T** and **R** states and that this alteration in quaternary structure is a consequence of specific amino acid interaction alterations.[39] In the study by Cherfils et al.,[39] 850 cycles of parallel energy minimization on the wild-type and the pAR5 mutant structures of ATCase yielded highly correlated movements between these struc-

**TABLE VII. Polar Contacts Involving the First Seven Residues of Chain *R*1 of CTP-Ligated T State ATCase***

| Atom pair | Distance (Å) |
|---|---|
| Met $N_1$—Tyr $O_{89}{}^{\eta}$ | 2.5 |
| Thr $O_2$—Asp $N_4$ | 2.6 |
| Thr $O_2{}^{\gamma}$—Lys $N_{129}{}^{\zeta\dagger}$ | 3.5 |
| Thr $O_2{}^{\gamma}$—Asn $O_{132}{}^{\delta 1\dagger}$ | 2.9 |
| Thr $O_2{}^{\gamma}$—His $N_3{}^{\delta 1}$ | 3.1 |
| Thr $O_2{}^{\gamma}$—Asn $O_{132}{}^{\dagger}$ | 3.2 |
| His $N_3{}^{\delta 1}$—Asn $O_{132}{}^{\dagger}$ | 3.1 |
| His $N_3{}^{\delta 1}$—Glu $O_{10}{}^{\epsilon 2}$ | 3.4 |
| His $N_3{}^{\epsilon 2}$—Asp $O_{133}{}^{\dagger}$ | 3.5 |
| Asp $O_4$—Glu $N_{10}$ | 3.3 |
| Asn $N_5$—*R*6 Gln $O_8$ | 2.9 |
| Asn $O_5$—Val $N_9$ | 3.4 |
| Asn $O_5{}^{\delta 1}$—Leu $N_7$ | 3.3 |
| Asn $N_5{}^{\delta 2}$—Gln $O_8$ | 2.9 |
| Lys $N_6$—R6 Glu $O_{10}{}^{\epsilon 1}$ | 3.3 |
| Lys $N_6{}^{\zeta}$—R6 Glu $O_{62}{}^{\epsilon 1}$ | 2.9 |
| Lys $O_6$—Gln $N_8$ | 3.5 |

*All atoms not otherwise delineated are constituents of *R*1.
†These interactions involve residues from an *r*130s loop of a neighboring molecule in the crystal.

tures, indicating that the mutant amino acid sequence could be fit to the native form without creating major steric conflicts and consequently major structural alterations. The main chain rms differences after energy minimization *between* the regulatory chains of pAR5 and native ATCase were equivalent to only one-fourth of the rms differences *within* each structure. Cherfils et al.[39] also demonstrated that the presence of carbamoyl phosphate shifted the X-ray scattering curve of the pAR5 mutant toward that of the **R** form, though carbamoyl phosphate has no effect on the X-ray scattering curve of wild-type ATCase.[78] Thus, the effects of the pAR5 mutation on the secondary structure of the regulatory chains are slight, and inspection of the scattering curve indicates that the new carboxy-terminal sequence of the mutant has decreased the stability of the **T** form of ATCase. Taken together, these functional observations and structural alterations suggested to Cherfils et al.[39] that the altered behavior of the pAR5 mutant involves a perturbation of the *C*1–*R*4 interface, the interface which crystal structure work first identified as critical to the homotropic transition.[25,29] The *R*1–*C*4 interface is related to the *C*1–*R*4 interface by a noncrystallographic 2-fold axis, i.e., these two interfaces are each ruptured with similar consequences in the **T** → **R** transition though individual amino acid contacts when comparing these two interfaces in any one state may be asymmetric. Therefore, the convention adopted here will employ "*C*1–*R*4 interface" when referring to the general consequences of this interface which unites a regulatory chain with a catalytic chain from the opposing catalytic trimer (see Fig. 1 and note that there are six such interfaces in the ATCase holoenzyme), while "*R*1–*C*4" will be used to describe one of the two specific classes of these interfaces (of which there are three in the ATCase holoenzyme).

The *C*1–*R*4 interface is extensive in the **T** form but absent in the **R** form.[29] One of the residues which participates in this interface is *r*Asn-111.[25] In the CTP-bound **T** state ATCase structure reported here, the two *r*Asn-111 residues of the asymmetric unit are distributed differently in the *C*1–*R*4 interface. Asn-111 of *R*1 forms an interaction with Ser-238 of the catalytic chain in the other trimer [*C*4; 3.0 Å($O_{238}{}^{\gamma}$, $O_{111}{}^{\delta 1}$)]. *c*Ser-238 is a component of the *c*240s loop which undergoes a large reorientation in the **T** → **R** transition. In the **T** state the *c*240s loop from one catalytic chain stacks side-by-side with a molecular 2-fold axis-related *c*240s loop in the other catalytic chain while in the **R** state the *c*240s loops stack on top of each other.[29] Such a rearrangement of the *c*240s loop occurs during the expansion of the molecule along the crystallographic 3-fold axis, and it is of cardinal importance in the maintenance of the expanded (**R**) state once it is assumed. Interestingly, in this **T** state *R*1 Asn-153 is positioned such that its $N^{\delta 2}$ is capable of forming a hydrogen bonded bridge connecting the main chain carbonyl oxygens of *R*1 Val-108 and *R*1 Val-150 (Fig. 5a). This bridge may be an important component of the stabilization of *R*1 Val-108 and those residues contiguous with it in the regulatory chain (especially *R*1 Asn-111). Therefore, it is tempting to speculate that the interaction between the side chain of *R*1 Asn-153 and the main chain carbonyl oxygen of *R*1 Val-108 may be an important component in correctly orienting *R*1 Asn-111 to participate in a hydrogen bond with *C*4 Ser-238 in the *R*1–*C*4 interface (Fig. 5b). The loss of this interaction in pAR5 would destabilize the *C*1–*R*4 interfaces tethering the two trimers of the holoenzyme together and would be expected to produce an enzyme with very little cooperativity and one which more easily assumed the **R** form after the addition of substrate.

Lending support to this interpretation of pAR5 is the observation made by Cherfils et al.[39] that after 850 cycles of parallel energy minimization one of the residues whose main chain atoms moved significantly in the pAR5 mutant relative to native ATCase was *r*Val-108. Furthermore, a recent site-directed mutant of ATCase[79] in which Ala was substituted for *r*Asn-111 was devoid of all cooperativity. The mutant's sedimentation coefficient was found to be equivalent to that of PALA-ligated ATCase, and the addition of PALA had no further effect on the mutant enzyme's sedimentation coefficient. These results indicate that the *r*Asn-111 → Ala ATCase mutant assumes the **R** form, consistent with the assertion that *r*Asn-111 is a critical component of the *C*1–*R*4 interface and that alter-

ations in it can create an enzyme with **R**-like homotropic behavior (i.e., an enzyme which is pAR5-like). Unlike *R*1 Asn-111, *R*6 Asn-111 makes no significant contacts with residues in the *c*240s loop [4.2 Å($N_{238}$, $O_{111}^{\delta 1}$)]. This asymmetry in contacts is either an artifact of packing in the crystal or another example of asymmetry in the molecule as it is found in the *P*321 crystal form.[28]

The recent work of Xi et al.[80] on the nature of the altered homotropic cooperative interactions in pAR5 and (by comparison and extension) the cooperative interactions in native ATCase is in accord with the role suggested above for *R*1 Asn-153. Elimination of the two carboxy-terminal residues of the regulatory chains of wild-type ATCase (which would be expected to disrupt the hydrogen bonded bridge formed by *R*1 Asn-153, *R*1 Val-150, and *R*1 Val-108) produces an enzyme functionally similar to pAR5, while addition of the carboxy-terminal residues Ala and Asn to pAR5 (which would be expected to restore the hydrogen bonded bridge now formed by *R*1 Asn-153, *R*1 Ala-150, and *R*1 Val-108) produces an enzyme functionally similar to wild-type **T** state. Xi et al.[80] showed that the *c*Arg-250 → Asn mutant of wild-type and the *r*Lys-28 → Asn mutant of pAR5 were functionally similar to the wild-type **T** state. Based on the structure reported here, it is not surprising that the *c*Arg-250 → Asn mutant behaves as wild-type **T** state—*c*Arg-250 does not form interactions which bridge the *C*1–*R*4 [*C*1: 6.9 Å($N_{250}^{\eta 2}$, $O_{152}$); *C*6: 9.3 Å($N_{250}^{\eta 1}$, $O_{153}^{1}$)] or *C*1–*C*4 interfaces. Xi et al.[80] may be correct when they suggest that in pAR5 the carboxy-terminus of the shortened regulatory chain now interacts with *r*Lys-28, though mutating *r*Lys-28 to a residue incapable of interacting with the carboxy-terminus (instead of substituting a charge-charge interaction for a charge-polar interaction) would provide more convincing evidence for its role in the functional behavior of pAR5.

In summary, the structure reported here evaluated in parallel with mutagenesis experiments indicates that a disturbance of the interaction between the side chains of *R*1 Asn-111 and *C*4 Ser-238 in the *R*1–*C*4 interface is responsible for the homotropic behavior of the pAR5 mutant of ATCase. The loss of the side chain interaction of these residues in the mutant occurs as a consequence of the mutant's shortened carboxy-terminus, which cannot participate in a critical hydrogen bonding network that it would otherwise form with the carbonyl oxygens of *R*1 Ala-150 and *R*1 Val-108. The alterations in the environment of *R*1 Val-108 are transmitted to the side chain of *R*1 Asn-111, destroying its interaction with the side chain of *C*4 Ser-238. It is the loss of this hydrogen bond that decreases the stability of the general *C*1–*R*4 interface which performs a pivotal role in the structural integrity and the homotropic cooperativity of the **T** form of the enzyme.

## Mechanism of Negative Cooperativity

Molecular asymmetry is present in the CTP-ligated *P*321 crystal form of ATCase.[28] Whether this asymmetry is ligand-induced or inherent in the ATCase molecule is not clear and cannot be distinguished based on the structure which forms the basis of this report. Further complicating the issue of asymmetry in the molecule is that these two types of asymmetry need not be mutually exclusive but, in fact, can coexist. In this section, a ligand-induced mechanism of negative cooperativity which unites the two nucleotide binding regions of the two regulatory chains which constitute the asymmetric unit is identified. Though the reorientations described here do suggest that at least some of the asymmetry observed in the CTP-ligated enzyme is ligand-induced, the aforementioned caveats must be acknowledged. The following potential molecular mechanism of ligand-induced negative cooperativity is based on a comparison between the unligated[27] and CTP-ligated **T** state forms of ATCase.[§§]

The binding of CTP in the allosteric site of chain *R*1 initiates a substantial reorientation of the side chain of *R*1 His-20: $N_{20}^{\delta 1}$ and $N_{20}^{\epsilon 2}$ are reoriented 3.3 and 5.6 Å relative to the unligated structure, respectively. The $N_{20}^{\epsilon 2}$ of the imidazole ring is brought within 2.8 Å of one of the terminal phosphate oxygens of CTP. The $\gamma$-$^{13}C$ enrichment of regulatory chain histidine residues and analysis with NMR[75] indicated that of the four histidine residues of the regulatory chain, one unidentified histidine experienced a chemical shift consistent with its participation in a direct interaction with CTP or ATP. The *r*His-20 → Ala mutant of ATCase[76] shows a 10-fold reduction in affinity for CTP relative to that of wild-type, providing further evidence that *r*His-20 is important in the binding of this nucleotide in the allosteric site. In the CTP-ligated **T** state ATCase structure, $N_{20}^{\epsilon 2}$ also interacts with one of the carboxylate oxygens of *R*1 Asp-19 [3.2 Å($N_{20}^{\epsilon 2}$,$O_{19}^{\delta 2}$)]. The other carboxylate oxygen of *R*1 Asp-19 interacts with the amino group of *R*1 Lys-56 [3.0 Å($O_{19}^{\delta 1}$,$N_{56}^{\zeta}$)], which in turn interacts with the hydroxyl of *R*1 Ser-50 [3.2 Å($N_{56}^{\zeta}$,$O_{50}^{\gamma}$)]. These interactions ensure the proper orientation of *R*1 His-20 so that contact is maintained between the side chain of *R*1 His-20 and a $\gamma$-phosphate oxygen of *R*1 CTP.

This reorientation of *R*1 His-20 requires the rupture of a charge-polar interaction between the carbonyl oxygen of *R*1 Glu-52 and $N_{20}^{\delta 1}$ of *R*1 His-20

[§§]Though there are reorientations of catalytic chain residues evident as the unligated enzyme binds CTP[81] (e.g., *C*1 $\Delta C_{229}^{\zeta}$—1.7 Å; *C*6 $\Delta C_{229}^{\zeta}$—3.0 Å), the only residue reorientations discussed in this section of the text of this report pertain to the mechanism of negative cooperativity as it is manifest in the regulatory chains of the enzyme. A more exhaustive discussion of nucleotide binding and its consequences on both the regulatory and catalytic chains will appear elsewhere.

(3.3 Å). As a result, the *r*50s loop undergoes substantial reorientation, the side chains of *R*1 Met-53 and *R*1 Ser-50 undergoing the greatest rearrangement. The side chain of *R*1 Met-53 moves away from the solvent exposed face of the *r*50s loop to enter the space vacated by *R*1 His-20 ($\Delta S_{53}{}^{\delta}$—4.7 Å). *R*1 Ser $O_{50}{}^{\gamma}$ moves 4.9 Å to bind to the amino group of *R*1 Lys-56. Although the $C^{\alpha}$ of *R*1 Arg-55 shifts by only 0.7 Å, the side chain reorients substantially to become interdigitated between the side chains of *R*1 Asn-47 and *R*6 Asp-39. The side chain rearrangements these three residues undergo when CTP is ligated to the enzyme may be described as motion by the side chain of *R*1 Arg-55 ($\Delta C_{55}{}^{\zeta}$—2.7 Å) with a consequent displacement of the side chain of *R*6 Asp-39 ($\Delta C_{39}{}^{\gamma}$—3.0 Å), while *R*1 Asn-47 remains consistently positioned ($\Delta C_{47}{}^{\gamma}$—0.5 Å) at this resolution (2.5 Å). In studies of ATCase ligated with PAM and malonate in the presence of CTP or ATP,[33] it was suggested that these residues might participate in some form of signal transduction from the allosteric site. Recent work has suggested a potential role for the *R*1–*R*6 interface in the heterotropic regulatory mechanism.[81] Comparison of structures of the CTP-ligated T form relative to the unligated T form of ATCase shows the loss of hydrogen bonds between the side chains of *R*6 Asp-39 and *R*1 Asn-47, *R*6 Asp-39 and *R*1 Arg-55, and *R*6 Asp-39 and *R*1 Gln-24 as CTP binds to the *R*1 allosteric site of the unligated enzyme. In exchange, interactions are formed in the CTP-ligated T state structure between the side chains of *R*1 Arg-55 and both *R*6 Asp-39 and *R*1 Asn-47. These side chain rearrangements continue as far as *R*6 Gln-40 ($\Delta C_{40}{}^{\delta}$—2.6 Å) and result in the rupture of hydrogen bonds between the side chains of *R*6 Gln-40 and *R*6 Asn-63 (Fig. 16 and Table VIII).

Though there are no significant main chain amino acid movements in the *R*6 *r*60s loop which can be identified at this resolution and though a comparison of the rms differences between the unligated[27] and CTP-ligated T state structures using the most stringent criterion available reveals that the reorientation of *R*6 Lys-60 can be subsumed by the intrinsic error in the coordinates (see below and Table IX), the amino group of *R*6 Lys-60 is reoriented 2.9 Å with respect to the unligated structure. The electron density in an $(|F_o| - |F_c|)e^{i\alpha_{calc}}$ omit map unequivocally establishes the correct orientation of *R*6 Lys-60 in both the unligated and CTP-ligated structures, suggesting that the estimated coordinate errors used when establishing the significance threshold may be higher than what is appropriate for *R*6 Lys-60. The method employing multiple refinements of the CTP-ligated T state structure described earlier in Results and Discussion defines a minimal coordinate error for *R*6 Lys-60 of 0.3 Å ($\sigma_{R6\ Lys\text{-}60}$ = 0.4 Å; $2\sigma_{R6\ Lys\text{-}60}$ = 0.9 Å), which implies that even though this residue does not fulfill the most stringent criterion for rearrangement, when only the minimal errors for this residue and the electron density accorded it by the data are considered its rearrangement is convincing.

Though the unequivocal establishment of the reorientation of *R*6 Lys-60 cannot be made, the position in which *R*6 Lys-60 refined eliminates its terminal amino group's contacts with the 2-keto and 2′-OH groups of *R*6 CTP. This asymmetry in the interactions between *r*Lys-60 and the 2-keto and 2′-hydroxyl moieties of CTP was evident in a previous crystal structure of the CTP-ligated T form of ATCase.[28] Furthermore, when the main chain atoms of chains *R*1 and *R*6 of the CTP-ligated structure are superimposed, the side chain of *R*1 Lys-60 is capable of interacting with *R*6 CTP (the relevant distances are both 3.2 Å for the interactions between *R*1 Lys $N_{60}{}^{\zeta}$ and the 2-keto and 2′-OH groups of *R*6 CTP). Though the reorientation of *R*6 Lys-60 has been described as a result of the aforementioned alterations in amino acid contacts, it is also conceivable that *R*6 Lys-60 may be oriented in this fashion due to inherent asymmetry in the molecule as found in the *P*321 crystal form. However, it has been shown that *r*Lys-60 is required for binding of CTP to the allosteric site of ATCase.[82] When *r*Lys-60 is mutated to an alanine,[82] the affinity of ATCase for CTP decreases 100-fold; this ratio is similar to the relative affinities of the two types of allosteric binding sites for CTP on the holoenzyme.[43] Interestingly, the *r*Lys-60 → Ala mutant could still be inhibited by CTP, implying that the interactions between *r*Lys-60 and CTP are responsible for binding CTP to the allosteric site and apparently not for conveying the resulting heterotropic inhibition when CTP is ligated to the enzyme.[82] Given the steric constraints within the nucleotide binding site, it is not surprising that the *r*Lys-60 → His mutant of ATCase[83] does not bind nucleotides.[¶¶]

A method analogous to Baldwin and Chothia's[84] was employed to determine the significance of all of the aforementioned rearrangements in the mechanism of ligand-induced negative cooperativity. Based on data published on a previous structure refinement of the CTP-ligated T form of ATCase,[28] the maximal rms errors in the coordinates of the regulatory chains are ≈0.7 Å. This value for the maximal rms error was utilized in the following calculations in order to ensure that all calculated movements were substantial by the most rigorous criterion available. Therefore, when homologous regions of the unligated and CTP-ligated regulatory chains are superimposed the maximal rms difference expected based on the errors in the coordinates

[¶¶]The location of *r*Lys-60 was incorrectly identified in this study.[83] It is located in the nucleotide binding site, *not* at the regulatory dimer interface.

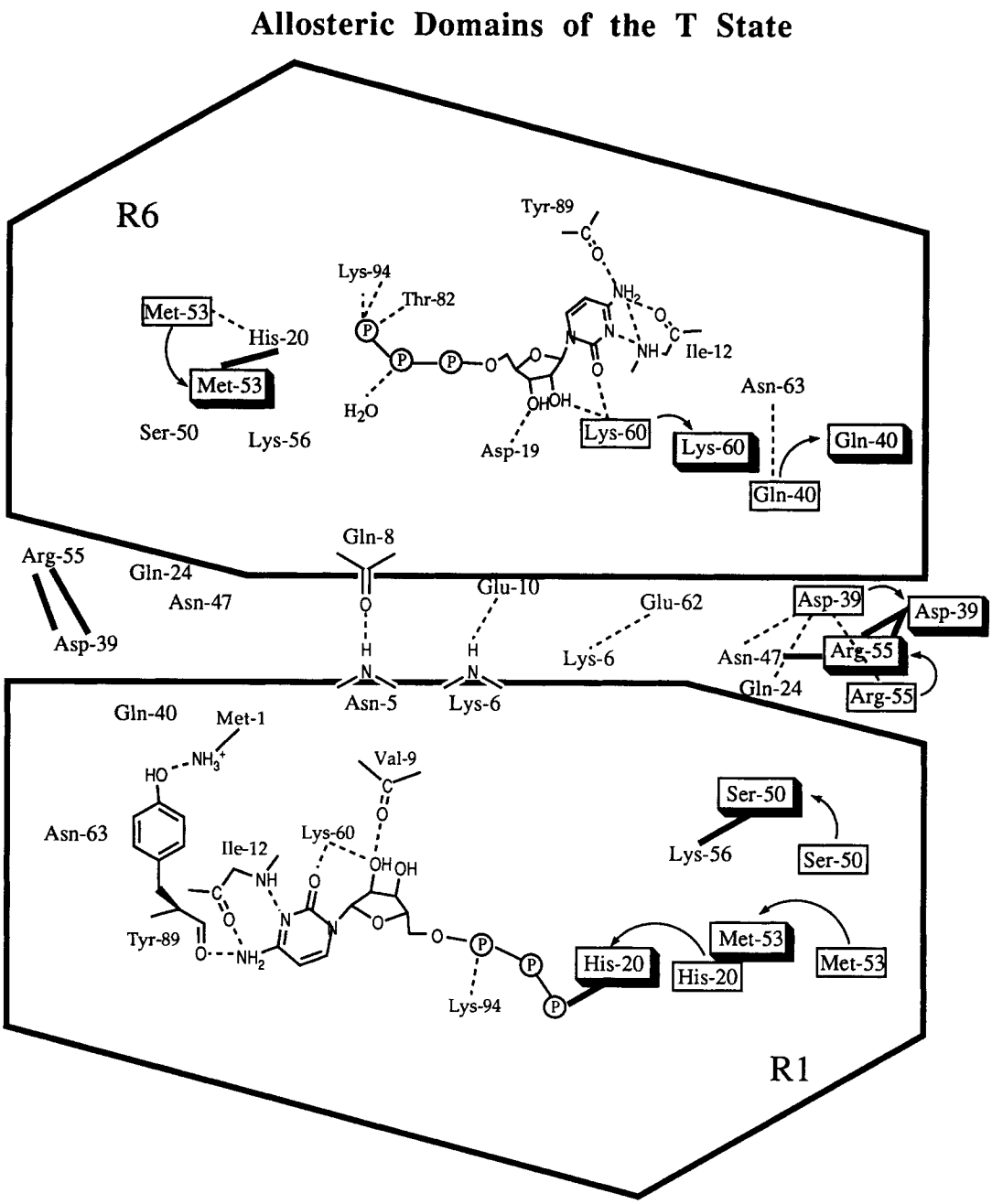


Fig. 16. Schematic diagram illustrating the interactions of CTP with residues in the allosteric site of T state ATCase (dashed lines) and the relevant interactions and displacements associated with selected residues of the proposed mechanism of negative cooperativity (see text). Unboxed residues of this mechanism undergo no significant movement as unligated T state ATCase[27] binds CTP, while boxed residues represent those which reorient as CTP binds to ATCase. Boxes which have not been highlighted correspond to residues in the unligated T state structure, and highlighted boxes represent residues associated with the CTP-ligated T state structure. Interactions pertinent to the mechanism of negative cooperativity that are evident in the CTP-ligated T state structure are indicated by boldface lines while selected interactions of the unligated structure are indicated by dashed lines. The 2 interactions between *R*6 Asp-39 and *R*1 Arg-55 of the unligated structure (Table VIII) are indicated by 1 dashed line. Interactions involving the first seven residues of *R*1 which span the molecular 2-fold axis are also indicated (dashed lines).

alone is 1.0 Å ($\sigma$). All main chain atoms in the asymmetric units of the unligated and CTP-ligated structures were superimposed, and the rms differences in the coordinates of the residues implicated in the mechanism described above were calculated. The results are summarized in Table IX. The significance threshold is $\sigma \geq 2.0$ Å for amino acid residue reorientation.[84] As is evident in Table IX, all of the

**TABLE VIII. Polar Contacts Pertinent to the Proposed Mechanism of Negative Cooperativity of CTP Binding to the Allosteric Sites of T State ATCase***

| Atom pair | Distance (Å) (unligated ATCase[27]) | Distance (Å) (CTP-ligated ATCase) | ΔDistance (Å) (Unl. → CTP) |
|---|---|---|---|
| Ser $O_{50}^{\gamma}$—Lys $N_{56}^{\zeta}$ | 5.1 | 3.2 | |
| *R*6 Asp $O_{39}^{\delta2}/O_{39}^{\delta1}$—Asn $N_{47}^{\delta2}$ | 3.9† | 5.1 | *R*6 $\Delta C_{39}^{\gamma}$—3.0‡ |
| *R*6 Asp $O_{39}^{\delta2}/O_{39}^{\delta1}$—Arg $N_{55}^{\epsilon}$ | 3.0 | 4.8 | |
| *R*6 Asp $O_{39}^{\delta1}$—Gln $N_{24}^{\epsilon2}$ | 3.3 | 4.6 | *R*6 $\Delta C_{39}^{\gamma}$—3.0‡ |
| Arg $N_{55}^{\eta1}$—*R*6 Asp $O_{39}^{\delta1}$ | 3.8 | 3.2 | $\Delta C_{55}^{\zeta}$—2.7‡ |
| Arg $N_{55}^{\eta2}$—*R*6 Asp $O_{39}^{\delta1}$ | 3.5 | 3.1 | $\Delta C_{55}^{\zeta}$—2.7‡ |
| Arg $N_{55}^{\eta2}$—Asn $O_{47}^{\delta1}$ | 5.7 | 2.9 | |
| *R*6 Asn $N_{63}^{\delta2}/O_{63}^{\delta1}$—*R*6 Gln $O_{40}^{\epsilon1}/N_{40}^{\epsilon2}$ | 3.1 | 6.3 | |

*All residues listed in this table are constituents of the regulatory chain of ATCase. Those atoms lacking a chain designation are from *R*1. Slashes are used to indicate that different atoms were selected to yield the interaction distances in the different structures. The atom on the left of the slash was used in the unligated ATCase interaction distance calculation. The atom on the right of the slash was utilized in the CTP-ligated ATCase interaction distance calculation.

†This atom pair is included in spite of having a hydrogen bond in the unligated structure which exceeds the upper limits of acceptability (3.5 Å) because the side chain atoms of Asn-47 may be rotated about $\chi^2$ in an $(|F_o| - |F_c|)e^{i\alpha_{calc}}$ omit map at 2.0σ until an acceptable hydrogen bond contact is achieved without sacrificing the fit of the residue in electron density.

‡All atom pairs which showed a relative interaction displacement of 1.5 Å or less as the unligated structure bound CTP contain a relevant absolute displacement to show that, in fact, significant *absolute* reorientation had occurred even if *relative* reorientation had not occurred (see Table IX).

**TABLE IX. rms Differences Between Unligated and CTP-Ligated T State Structures For Residues Implicated in the Mechanism of Negative Cooperativity***

| Residue | rms difference (Å) for the entire residue | rms difference (Å) for main chain atoms† | rms difference (Å) for side chain atoms |
|---|---|---|---|
| His-20 | 3.0 (1.5) | 0.3 (0.3) | 3.8 (1.9) |
| Gln-24 | 0.5 (1.1) | 0.3 (0.6) | 0.5 (1.4) |
| Asn-47 | 0.4 (0.5) | 0.2 (0.3) | 0.5 (0.6) |
| Ser-50 | 4.1 (1.3) | 3.0 (1.3) | 4.5 (1.3) |
| Met-53 | 2.8 (3.1) | 0.5 (1.3) | 3.9 (4.1) |
| Arg-55 | 2.0 (1.1) | 0.7 (0.8) | 2.5 (1.3) |
| Lys-56 | 0.4 (0.8) | 0.3 (0.4) | 0.5 (0.9) |
| Asp-39 | 2.4 (1.6) | 0.7 (0.7) | 3.2 (2.2) |
| Gln-40 | 2.0 (0.6) | 0.6 (0.5) | 2.7 (0.6) |
| Asn-63 | 0.7 (0.9) | 0.6 (0.7) | 0.8 (0.7) |
| Lys-60 | 1.3 (0.5) | 0.2 (0.5) | 1.7 (0.5) |

*All nonparenthetical values refer to the residues which constitute the *R*1 → *R*6 pathway. All results in parentheses refer to residues of the *R*6 → *R*1 pathway.

†$(N_i, C_i^{\alpha}, C_i)$ were used in the calculation of main chain rms values.

residue reorientations which were implicated in the mechanism of negative cooperativity (except *R*6 Lys-60) satisfied this significance criterion. Furthermore, the molecular mechanism proposed for negative cooperativity in the binding of CTP to T state ATCase is exclusively dependent upon side chain reorientations, the average residue main chain rms difference being only 0.7 Å (Table IX). Any potentially significant main chain movements are invisible at this resolution (2.5 Å).

If the mechanism proposed above for the negative cooperativity of CTP binding to the allosteric sites of T state ATCase is correct, the interactions which constitute this mechanism should be nonuniformly distributed among the allosteric sites in the asymmetric unit of the enzyme. In other words, if the changes which are being propagated from site *R*1 to site *R*6 are ligand-induced and result in the two different classes of binding sites on T state ATCase for CTP, similar reorientations should not be found in the analogous pathway linking the *R*6 site to the *R*1 site. There were no major reorientations of the side chains of *R*6 Arg-55 ($\Delta C_{55}^{\zeta}$—1.1 Å), *R*6 Asn-47 ($\Delta C_{47}^{\gamma}$—0.6 Å), or *R*1 Asp-39 ($\Delta C_{39}^{\gamma}$—1.7 Å) evident as CTP binds to the unligated T form of ATCase. Among these three residues only *R*6 Arg-55 and *R*1 Asp-39 interact with one another [3.5 Å($N_{55}^{\eta2}$,$O_{39}^{\delta1}$); 3.0 Å($N_{55}^{\eta1}$,$O_{39}$)]. With the exception of the side chain of *R*6 Met-53 which reorients while maintaining an interaction with the side chain of *R*6 His-20 [3.3 Å [unligated structure] → 3.4 Å [CTP-ligated ATCase structure] ($N_{20}^{\epsilon2}$,$S_{53}^{\delta}$)], none of the residues in the *R*6 → *R*1 pathway reorients significantly as assessed by the method of Baldwin and Chothia[84] (Table IX). In short, the substantial amino acid side chain movements described above which lead from the *R*1 CTP allosteric site to the *R*6 CTP allosteric site and culminate in the possible reorientation of *R*6 Lys-60 such that it is incapable of binding CTP are not reproduced when one views the analogous residues from the *R*6 CTP allosteric site to the *R*1 CTP allosteric site.

A preliminary T state structure of ATCase ligated with CTP and UTP at pH 7.0 and excluding solvent[71] showed striking conformational similarities to the CTP-ligated T state ATCase structure, in spite of differences in pH and uncertainties concern-

ing the identity of the nucleotides in each nucleotide binding site. The same reorientations, though less extensive, of the side chains of *R*6 Asp-39 ($\Delta C_{39}{}^{\gamma}$–3.5 Å) and *R*1 Arg-55 ($\Delta C_{55}{}^{\zeta}$—1.6 Å) occur, resulting in the interdigitation of the side chain of *R*1 Arg-55 between the side chains of *R*1 Asn-47 and *R*6 Asp-39. As in the CTP-ligated T state ATCase structure described above, these changes are associated with a destruction of the link between the side chains of *R*6 Gln-40 and *R*6 Asn-63. Furthermore, the CTP+UTP structure reveals a heterogeneity in the contacts formed between *r*Lys-60 and the nucleotides in the nucleotide binding site. The *R*1 Lys-60 has strong interactions with a ribose hydroxyl and the group in the 2-keto position of the nucleotide (2.7 and 3.2 Å, respectively), while the *R*6 Lys-60 only interacts weakly (3.4 Å) with the group in the 2-keto position of the nucleotide. Therefore, the asymmetry in the interactions of *R*1 Lys-60 and *R*6 Lys-60 with CTP in the CTP-ligated T form of the enzyme also occurs in the CTP+UTP T state ATCase structure at neutral pH.

In conclusion, the binding of CTP to the *R*1 allosteric domain of unligated T state ATCase initiates a series of amino acid side chain reorientations which are propagated to the *R*6 allosteric domain binding site and culminates in a reorientation of *R*6 Lys-60. This reorientation of *R*6 Lys-60 results in a loss of the critical interactions which *R*1 Lys-60 forms with CTP in the *R*1 site, and consequently, the reorientation of *R*6 Lys-60 results in a reduced affinity for CTP in the *R*6 site relative to the *R*1 site. As expected, these rearrangements are not evident when the analogous residues which originate in the *R*6 site and link it with the *R*1 site are analyzed. Finally, the seminal aspects of this molecular pathway are also evident in a preliminary T state structure of ATCase ligated with CTP+UTP at pH 7.0.[71] Mutagenesis work on the residues outlined above will serve to further delineate and modify the static view of this pathway which has been derived from the crystal structures.

## ACKNOWLEDGMENTS

The authors thank E.R. Kantrowitz for providing purified ATCase for this study. H. Kim and R.C. Stevens are recognized for providing helpful comments on the manuscript, and H.M. Ke is acknowledged for generous help with the data collection. R.P.K. thanks Prof. Farish A. Jenkins, Jr. and Dr. Roger Mark of Harvard Medical School/M.I.T., and Dr. Joseph Perpich of the Howard Hughes Medical Institute for their counsel, advice, and encouragement. This work was supported by a National Institutes of Health Grant (GM 06920) to W.N.L. and a Howard Hughes Medical Institute Medical Student Research Training Fellowship to R.P.K.

## REFERENCES

1. Jones, M.E., Spector, L., Lipmann, F. Carbamyl phosphate, the carbamyl donor in enzymatic citrulline synthesis. J. Am. Chem. Soc. 77:819–820, 1955.
2. Reichard, P., Hanshoff, G. Aspartate carbamyl transferase from *Escherichia coli*. Acta Chem. Scand. 10:548–566, 1956.
3. Kantrowitz, E.R., Lipscomb, W.N. *Escherichia coli* aspartate transcarbamylase: The relations between structure and function. Science (Washington, D.C.) 241:669–674, 1988.
4. Kantrowitz, E.R., Lipscomb, W.N. *Escherichia coli* aspartate transcarbamoylase: The molecular basis for a concerted allosteric transition. Trends Biochem. Sci. 15:53–59, 1990.
5. Stevens, R.C., Chook, Y.M., Cho, C.Y., Lipscomb, W.N., Kantrowitz, E.R. *Escherichia coli* aspartate carbamoyltransferase: The probing of crystal structure analysis via site-specific mutagenesis. Protein Eng. 4:391–408, 1991.
6. Kantrowitz, E.R., Pastra-Landis, S.C., Lipscomb, W.N. *E. coli* aspartate transcarbamylase: Part I: Catalytic and regulatory functions. Trends Biochem. Sci. 5:124–128, 1980.
7. Kantrowitz, E.R., Pastra-Landis, S.C., Lipscomb, W.N. *E. coli* aspartate transcarbamylase: Part II: Structure and allosteric interactions. Trends Biochem. Sci. 5:150–153, 1980.
8. Beckwith, J.R., Pardee, A.B., Austrian, R., Jacob, F. Coordination of the synthesis of the enzymes in the pyrimidine pathway of *E. coli*. J. Mol. Biol. 5:618–634, 1962.
9. Gerhart, J.C., Pardee, A.B. The enzymology of control by feedback inhibition. J. Biol. Chem. 237:891–896, 1962.
10. Bethell, M.R., Smith, K.E., White, J.S., Jones, M.E. Carbamyl phosphate: An allosteric substrate for aspartate transcarbamylase of *Escherichia coli*. Proc. Natl. Acad. Sci. U.S.A. 60:1442–1449, 1968.
11. Wild, J.R, Loughrey-Chen, S.J., Corder, T.S. In the presence of CTP, UTP becomes an allosteric inhibitor of aspartate transcarbamoylase. Proc. Natl. Acad. Sci. U.S.A. 86: 46–50, 1989.
12. Warren, S.G., Edwards, B.F.P., Evans, D.R., Wiley, D.C., Lipscomb, W.N. Aspartate transcarbamoylase from *Escherichia coli:* Electron density at 5.5 Å resolution. Proc. Natl. Acad. Sci. U.S.A. 70:1117–1121, 1973.
13. Edwards, B.F.P., Evans, D.R., Warren, S.G., Monaco, H.L., Landfear, S.M., Eisele, G., Crawford, J.L., Wiley, D.C., Lipscomb, W.N. Complex of aspartate carbamoyltransferase from *Escherichia coli* with its allosteric inhibitor, cytidine triphosphate: Electron density at 5.9-Å resolution. Proc. Natl. Acad. Sci. U.S.A. 71:4437–4441, 1974.
14. Weber, K. New structural model of *E. coli* aspartate transcarbamylase and the amino-acid sequence of the regulatory polypeptide chain. Nature (London) 218:1116–1119, 1968.
15. Wiley, D.C., Lipscomb, W.N. Crystallographic determination of symmetry of aspartate transcarbamylase. Nature (London) 218:1119–1121, 1968.
16. Gerhart, J.C., Schachman, H.K. Distinct subunits for the regulation and catalytic activity of aspartate transcarbamylase. Biochemistry 4:1054–1062, 1965.
17. Gerhart, J.C., Schachman, H.K. Allosteric interactions in aspartate transcarbamylase. II. Evidence for different conformational states of the protein in the presence and absence of specific ligands. Biochemistry 7:538–552, 1968.
18. Howlett, G.J., Schachman, H.K. Allosteric regulation of aspartate transcarbamoylase. Changes in the sedimentation coefficient promoted by the bisubstrate analogue *N*-(phosphonacetyl)-L-aspartate. Biochemistry 16:5077–5083, 1977.
19. Moody, M.F., Vachette, P., Foote, A.M. Changes in the X-ray solution scattering of aspartate transcarbamylase following the allosteric transition. J. Mol. Biol. 133:517–532, 1979.
20. Monaco, H.L., Crawford, J.L., Lipscomb, W.N. Three-dimensional structures of aspartate carbamoyltransferase from *Escherichia coli* and of its complex with cytidine triphosphate. Proc. Natl. Acad. Sci. U.S.A. 75:5276–5280, 1978.
21. Ladner, J.E., Kitchell, J.P., Honzatko, R.B., Ke, H.M., Volz, K.W., Kalb (Gilboa), A.J., Ladner, R.C., Lipscomb, W.N. Gross quaternary changes in aspartate carbamoyl-

transferase are induced by the binding of *N*-(phosphonacetyl)-L-aspartate: A 3.5-Å resolution study. Proc. Natl. Acad. Sci. U.S.A. 79:3125–3128, 1982.
22. Howlett, G.J., Blackburn, M.N., Compton, J.G., Schachman, H.K. Allosteric regulation of aspartate transcarbamoylase. Analysis of the structural and functional behavior in terms of a two-state model. Biochemistry 16: 5091–5099, 1977.
23. Collins, K.D., Stark, G.R. Aspartate transcarbamylase. Interaction with the transition state analogue *N*-(phosphonacetyl)-L-aspartate. J. Biol. Chem. 246:6599–6605, 1971.
24. Foote, J., Schachman, H.K. Homotropic effects in aspartate transcarbamoylase. What happens when the enzyme binds a single molecule of the bisubstrate analog *N*-phosphonacetyl-L-aspartate? J. Mol. Biol. 186:175–184, 1985.
25. Honzatko, R.B., Crawford, J.L., Monaco, H.L., Ladner, J.E., Edwards, B.F.P., Evans, D.R., Warren, S.G., Wiley, D.C., Ladner, R.C., Lipscomb, W.N. Crystal and molecular structures of native and CTP-liganded aspartate carbamoyltransferase from *Escherichia coli*. J. Mol. Biol. 160: 219–263, 1982.
26. Ke, H.M., Honzatko, R.B., Lipscomb, W.N. Structure of unligated aspartate carbamoyltransferase of *Escherichia coli* at 2.6-Å resolution. Proc. Natl. Acad. Sci. U.S.A. 81: 4037–4040, 1984.
27. Stevens, R.C., Gouaux, J.E., Lipscomb, W.N. Structural consequences of effector binding to the T state of aspartate carbamoyltransferase: Crystal structures of the unligated and ATP- and CTP-complexed enzymes at 2.6-Å resolution. Biochemistry 29:7691–7701, 1990.
28. Kim, K.H., Pan, Z., Honzatko, R.B., Ke, H.M., Lipscomb, W.N. Structural asymmetry in the CTP-liganded form of aspartate carbamoyltransferase from *Escherichia coli*. J. Mol. Biol. 196:853–875, 1987.
29. Krause, K.L., Volz, K.W., Lipscomb, W.N. 2.5 Å structure of aspartate carbamoyltransferase complexed with the bisubstrate analog *N*-(phosphonacetyl)-L-aspartate. J. Mol. Biol. 193:527–553, 1987.
30. Ke, H.M., Lipscomb, W.N., Cho, Y., Honzatko, R.B. Complex of *N*-phosphonacetyl-L-aspartate with aspartate carbamoyltransferase. X-ray refinement, analysis of conformational changes and catalytic and allosteric mechanisms. J. Mol. Biol. 204:725–747, 1988.
31. Gouaux, J.E., Lipscomb, W.N. Three-dimensional structure of carbamoyl phosphate and succinate bound to aspartate carbamoyltransferase. Proc. Natl. Acad. Sci. U.S.A. 85:4205–4208, 1988.
32. Gouaux, J.E., Lipscomb, W.N. Crystal structures of phosphonoacetamide ligated T and phosphonoacetamide and malonate ligated R states of aspartate carbamoyltransferase at 2.8-Å resolution and neutral pH. Biochemistry 29:389–402, 1990.
33. Gouaux, J.E., Stevens, R.C., Lipscomb, W.N. Crystal structures of aspartate carbamoyltransferase ligated with phosphonoacetamide, malonate, and CTP or ATP at 2.8-Å resolution and neutral pH. Biochemistry 29:7702–7715, 1990.
34. Stevens, R.C., Lipscomb, W.N. Allosteric control of quaternary states in *E. coli* aspartate transcarbamylase. Biochem. Biophys. Res. Commun. 171:1312–1318, 1990.
35. Gao, J., Kuczera, K., Tidor, B., Karplus, M. Hidden thermodynamics of mutant proteins: A molecular dynamics analysis. Science (Washington, D.C.) 244:1069–1072, 1989.
36. Feller, A., Pierard, A., Glansdorff, N., Charlier, D., Crabeel, M. Mutation of gene encoding regulatory polypeptide of aspartate carbamoyltransferase. Nature (London) 292: 370–373, 1981.
37. Cunin, R., Jacobs, A., Charlier, D., Crabeel, M., Hervé, G., Glansdorff, N., Piérard, A. Structure–function relationship in allosteric aspartate carbamoyltransferase from *Escherichia coli*. I. Primary structure of a *pyrI* gene encoding a modified regulatory subunit. J. Mol. Biol. 186:707–713, 1985.
38. Ladjimi, M.M., Ghellis, C., Feller, A., Cunin, R., Glansdorff, N., Piérard, A., Hervé, G. Structure-function relationship in allosteric aspartate carbamoyltransferase from *Escherichia coli*. II. Involvement of the C-terminal region of the regulatory chain in homotropic and heterotropic interactions. J. Mol. Biol. 186:715–724, 1985.
39. Cherfils, J., Vachette, P., Tauc, P., Janin, J. The pAR5 mutation and the allosteric mechanism of *Escherichia coli* aspartate carbamoyltransferase. EMBO J. 6:2843–2847, 1987.
40. Brünger, A.T., Kuriyan, J., Karplus, M. Crystallographic *R* factor refinement by molecular dynamics. Science (Washington, D.C.) 235:458–460, 1987.
41. Honzatko, R.B., Lipscomb, W.N. Interactions of phosphate ligands with *Escherichia coli* aspartate carbamoyltransferase in the crystalline state. J. Mol. Biol. 160:265–286, 1982.
42. Honzatko, R.B., Lipscomb, W.N. Interactions of metal-nucleotide complexes with aspartate carbamoyltransferase in the crystalline state. Proc. Natl. Acad. Sci. U.S.A. 79: 7171–7174, 1982.
43. Suter, P., Rosenbusch, J.P. Asymmetry of binding and physical assignments of CTP and ATP sites in aspartate transcarbamoylase. J. Biol. Chem. 252:8136–8141, 1977.
44. Matsumoto, S., Hammes, G.G. An equilibrium binding study of the interaction of aspartate transcarbamylase with cytidine 5′-triphosphate and adenosine 5′-triphosphate. Biochemistry 12:1388–1394, 1973.
45. Suter, P., Rosenbusch, J.P. Determination of ligand binding: Partial and full saturation of aspartate transcarbamylase. Applicability of a filter assay to weakly binding ligands. J. Biol. Chem. 251:5986–5991, 1976.
46. London, R.E., Schmidt, P.G. A nuclear magnetic resonance study of the interaction of inhibitory nucleosides with *Escherichia coli* aspartate transcarbamylase and its regulatory subunit. Biochemistry 13:1170–1179, 1974.
47. Tondre, C., Hammes, G.G. Interaction of aspartate transcarbamylase with 5-bromocytidine 5′-tri-, di-, and monophosphates. Biochemistry 13:3131–3136, 1974.
48. Gouaux, J.E., Lipscomb, W.N., Middleton, S.A., Kantrowitz, E.R. Structure of a single amino acid mutant of aspartate carbamoyltransferase at 2.5-Å resolution: Implications for the cooperative mechanism. Biochemistry 28: 1798–1803, 1989.
49. Sobottka, S.E., Cornick, G.G., Kretsinger, R.H., Rains, R.G., Stephens, W.A., Weissman, L.J. A MWPC X-ray diffractometer facility for protein crystallography. Nucl. Instrum. Methods 220:575–581, 1984.
50. Fox, G.C., Holmes, K.C. An alternative method of solving the layer scaling equations of Hamilton, Rollett and Sparks. Acta Crystallogr. 20:886–891, 1966.
51. Brünger, A.T. "X-PLOR Manual, Version 1.5." New Haven: Yale University, 1988.
52. Powell, M.J.D. Restart procedures for the conjugate gradient method. Math. Program. 12:241–254, 1977.
53. Ten Eyck, L.F. Crystallographic fast fourier transforms. Acta Crystallogr., Sect. A: Found. Crystallogr. 29:183–191, 1973.
54. Ten Eyck, L.F. Efficient structure-factor calculation for large molecules by the fast fourier transform. Acta Crystallogr., Sect. A: Found. Crystallogr. 33:486–492, 1977.
55. Jones, T.A. FRODO: A graphics fitting program for macromolecules. In: "Computational Crystallography." D. Sayre, ed. London: Oxford University Press, 1982: 303–317.
56. Pflugrath, J.W., Saper, M.A., Quiocho, F.A. New generation graphics system for molecular modeling. In: "Methods and Applications in Crystallographic Computing." S.R. Hall, T. Ashida, eds. Oxford: Clarendon Press, 1984: 404–407.
57. Janin, J., Wodak, S., Levitt, M., Maigret, B. Conformation of amino acid side-chains in proteins. J. Mol. Biol. 125: 357–386, 1978.
58. Weis, W.I., Brünger, A.T. Crystallographic refinement by simulated annealing. In: "Molecular Simulation and Protein Crystallography: Proceedings of the Joint CCP4/CCP5 Study Weekend 27–28 January, 1989." J. Goodfellow, K. Henrick, R. Hubbard, comps. England: Science & Engineering Research Council, 1989: 16–28.
59. Ramachandran, G.N., Ramakrishnan, C., Sasisekharan, V. Stereochemistry of polypeptide chain configurations. J. Mol. Biol. 7:95–99, 1963.
60. IUPAC-IUB Commission on Biochemical Nomenclature. Abbreviations and symbols for the description of the conformation of polypeptide chains. Tentative rules (1969). Biochemistry 9:3471–3479, 1970.

61. Artymiuk, P.J., Blake, C.C.F. Refinement of human lysozyme at 1.5 Å resolution. Analysis of non-bonded and hydrogen-bond interactions. J. Mol. Biol. 152:737–762, 1981.
62. Bhat, T.N., Cohen, G.H. *OMITMAP:* An electron density map suitable for the examination of errors in a macromolecular model. J. Appl. Crystallogr. 17:244–248, 1984.
63. Bhat, T.N. Calculation of an OMIT map. J. Appl. Crystallogr. 21:279–281, 1988.
64. Blundell, T.L., Johnson, L.N. "Protein Crystallography." Orlando: Academic Press, 1976.
65. Luzzati, P.V. Traitement statistique des erreurs dans la determination des structures cristallines. Acta Crystallogr. 5:802–810, 1952.
66. Kuriyan, J., Karplus, M., Petsko, G.A. Estimation of uncertainties in X-ray refinement results by use of perturbed structures. Proteins: Struct., Funct., Genet. 2:1–12, 1987.
67. Brünger, A.T. Crystallographic refinement by simulated annealing. Application to a 2.8 Å resolution structure of aspartate aminotransferase. J. Mol. Biol. 203:803–816, 1988.
68. Kabsch, W. A solution for the best rotation to relate two sets of vectors. Acta Crystallogr., Sect. A: Found. Crystallogr. 32:922–923, 1976.
69. Xu, W., Kantrowitz, E.R. Function of serine-52 and serine-80 in the catalytic mechanism of *Escherichia coli* aspartate transcarbamoylase. Biochemistry 30:2535–2542, 1991.
70. Stebbins, J.W., Xu, W., Kantrowitz, E.R. Three residues involved in binding and catalysis in the carbamyl phosphate binding site of *Escherichia coli* aspartate transcarbamylase. Biochemistry 28:2592–2600, 1989.
71. Stevens, R.C., Cho, C., Lipscomb, W.N. Preliminary results.
72. Cantor, C.R., Schimmel, P.R. "Biophysical Chemistry. Part I: The Conformation of Biological Macromolecules." San Francisco: W.H. Freeman, 1980.
73. Miller, S.K., Marzilli, L.G., Dörre, S., Kollat, P., Stigler, R.-D., Stezowski, J.J. Models for the interaction of $Zn^{2+}$ with DNA. Syntheses and X-ray structural characterizations of two polymeric tetrahedral zinc complexes of monomethyl phosphate esters of cytidine and deoxycytidine 5′-monophosphate nucleotides. Inorg. Chem. 25:4272–4277, 1986.
74. Wacks, D.B., Schachman, H.K. $^{19}F$ nuclear magnetic resonance studies of fluorotyrosine-labeled aspartate transcarbamoylase. Properties of the enzyme and its catalytic and regulatory subunits. J. Biol. Chem. 260:11651–11658, 1985.
75. Moore, A.C., Browne, D.T. Binding of regulatory nucleotides to aspartate transcarbamylase: Nuclear magnetic resonance studies of selectively enriched carbon-13 regulatory subunit. Biochemistry 19:5768–5773, 1980.
76. Zhang, Y., Kantrowitz, E.R. Probing the regulatory site of *Escherichia coli* aspartate transcarbamoylase by site-specific mutagenesis. Biochemistry 31:792–798, 1992.
77. Xi, X.G., van Vliet, F., Ladjimi, M.M., de Wannemaeker, B., de Staercke, C., Glansdorff, N., Piérard, A., Cunin, R., Hervé, G. Heterotropic interactions in *Escherichia coli* aspartate transcarbamylase. Subunit interfaces involved in CTP inhibition and ATP activation. J. Mol. Biol. 220:789–799, 1991.
78. Hervé, G., Moody, M.F., Tauc, P., Vachette, P., Jones, P.T. Quaternary structure changes in aspartate transcarbamylase studied by X-ray solution scattering. Signal transmission following effector binding. J. Mol. Biol. 185:189–199, 1985.
79. Eisenstein, E., Markby, D.W., Schachman, H.K. Changes in stability and allosteric properties of aspartate transcarbamoylase resulting from amino acid substitutions in the zinc-binding domain of the regulatory chains. Proc. Natl. Acad. Sci. U.S.A. 86:3094–3098, 1989.
80. Xi, X.G., Van Vliet, F., Ladjimi, M.M., De Wannemaeker, B., De Staercke, C., Piérard, A., Glansdorff, N., Hervé, G., Cunin, R. Co-operative interactions between the catalytic sites in *Escherichia coli* aspartate transcarbamylase. Role of the C-terminal region of the regulatory chains. J. Mol. Biol. 216:375–384, 1990.
81. Stevens, R.C., Lipscomb, W.N. A molecular mechanism for pyrimidine and purine nucleotide control of aspartate transcarbamoylase. Proc. Natl. Acad. Sci. U.S.A. 89:5281–5285, 1992.
82. Zhang, Y., Kantrowitz, E.R. Lysine-60 in the regulatory chain of *Escherichia coli* aspartate transcarbamoylase is important for the discrimination between CTP and ATP. Biochemistry 28:7313–7318, 1989.
83. Wente, S.R., Schachman, H.K. Different amino acid substitutions at the same position in the nucleotide-binding site of aspartate transcarbamoylase have diverse effects on the allosteric properties of the enzyme. J. Biol. Chem. 266: 20833–20839, 1991.
84. Baldwin, J., Chothia, C. Haemoglobin: The structural changes related to ligand binding and its allosteric mechanism. J. Mol. Biol. 129:175–220, 1979.